

Fiber Composites of Metal–Organic Frameworks

Kaikai Ma, Karam B. Idrees, Florencia A. Son, Rodrigo Maldonado, Megan C. Wasson, Xuan Zhang, Xingjie Wang, Elissa Shehayeb, Areej Merhi, Bilal R. Kaafarani, Timur Islamoglu, John H. Xin,* and Omar K. Farha*



Cite This: *Chem. Mater.* 2020, 32, 7120–7140



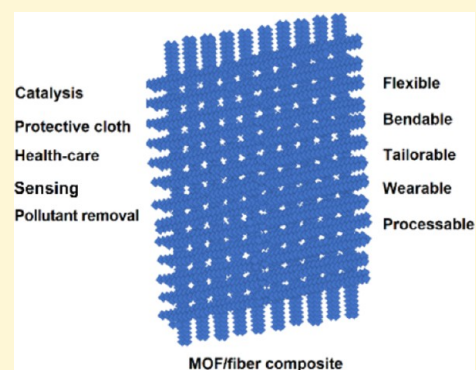
Read Online

ACCESS |

Metrics & More

Article Recommendations

ABSTRACT: The high chemical and structural diversity of metal–organic frameworks (MOFs), which are porous crystalline materials, has attracted significant academic and industrial interest. However, the poor processability of MOF powders limits their full potential in practical applications. Toward this end, MOF-based composite materials increase the framework robustness and subsequent utility. Among these hybrid materials, MOF composites prepared on commercially available textile fibers offer the high flexibility needed for important applications—such as heterogeneous catalysis, chemical sensing, pollutant removal, and drug release—while maintaining the functional properties of MOFs. The ability to further tailor these composites' shapes for incorporation into industrial equipment increases their potential in applications such as adsorption devices and protective gears. In this Review, we summarize recently reported MOF/fiber fabrication methods and applications. Our discussion on the advancements and remaining issues of these production methods segues into several highlighted applications of MOF/fiber composites, especially within adsorption devices and protective gears.



1. INTRODUCTION

Metal–organic frameworks (MOFs), also termed porous coordination polymers (PCPs), are a promising class of porous crystalline frameworks that form through the self-assembly of the inorganic nodes and organic linkers.^{1–5} Tuning the frameworks' inorganic and organic building blocks accesses a multitude of two- and three-dimensional topologies, each with its own specific set of physical and chemical properties (Figure 1). MOFs feature ultrahigh porosity, which can reach up to 90% free volume as well as high internal surface areas, reaching as high as 7000 m² g⁻¹.^{6,7} For these reasons, MOFs have shown great promise in a myriad of applications including, but not limited to, gas storage and separation,^{7–12} catalysis,^{13–17} pollutant control,^{18–21} and chemical sensing.^{22,23}

Typical MOF syntheses yield fine powdered materials with nano- to micron-sized particles. While powdered MOFs are amenable to academic research studies, their implementation in industrial settings, such as for gas storage and separation applications, require more robust materials that can be incorporated into existing equipment. Therefore, the integration of MOF powders onto a supporting material creates a more processable MOF-based composite better suited for practical applications.^{24–26} Prior work demonstrated successful MOF immobilization on a versatile series of substrates including membranes,²⁷ carbon nanotubes,²⁸ plastic films,²⁹ foams,³⁰ ceramics,^{31,32} metals,³³ and textile fibers.^{34–67} In addition to tuning chemical diversity, high porosity, and crystallinity via

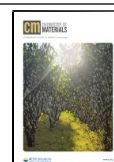
MOF structural components, the choice in supporting substrate can alter the flexibility, robustness, and processability in the MOF-based composite. The rational combination of a support and MOF yields mechanical properties and functionalities unobtainable in MOF powders alone that meet the requirements of a targeted application.

Among the aforementioned substrates for MOF-based composites, flexible textile fibers are inexpensive and abundant. Tuning the polymer composition, fiber thickness, permeability, porosity, and flexural rigidity subsequently permits us to target ideal properties for individual textiles. Reported MOF/fiber composites utilized the following natural fibers, cotton^{29,55,59} and silk,^{35,40,46} as well as the following synthetic polymeric fibers: poly(methyl methacrylate) (PMMA),³⁴ nylon,^{49,54} polyester (PET),³⁸ polystyrene (PS),⁴¹ polyvinylidene difluoride (PVDF),^{47,62} polypropylene (PP),^{39,43,50,57,63,68} and polyacrylonitrile (PAN).^{44,43,62} Thus, the functionalization of these highly flexible supports with an incorporated MOF tuned for a specific property yields composites suitable for a variety of either

Received: June 7, 2020

Revised: August 12, 2020

Published: August 26, 2020



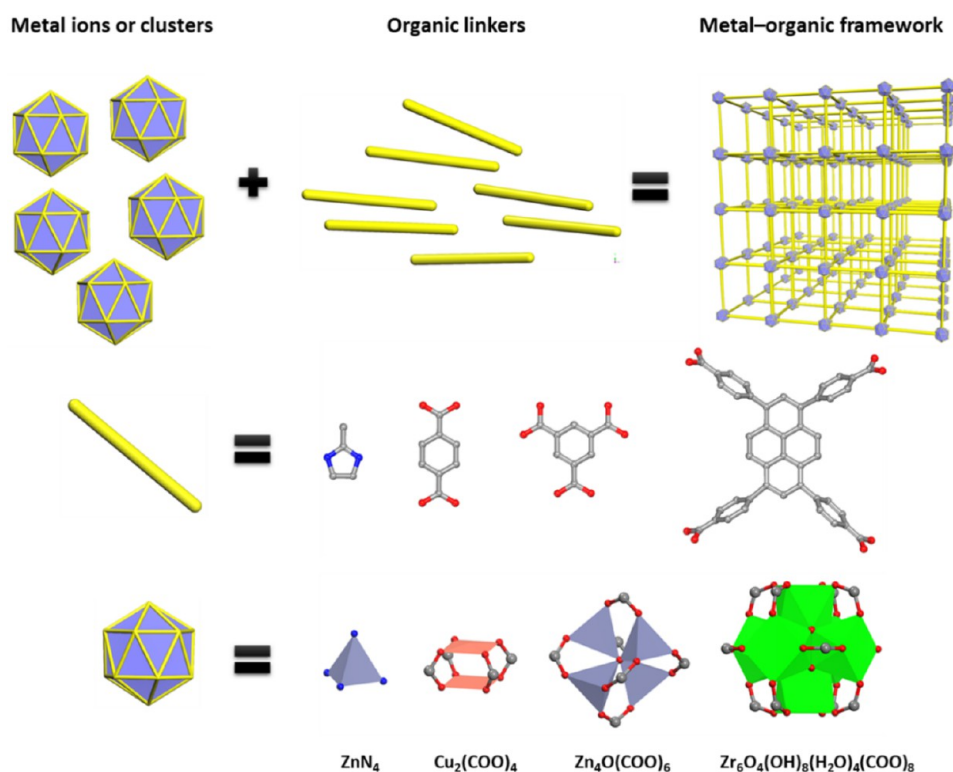


Figure 1. Depiction of MOF self-assembly through metal ions or cluster and organic linker.

liquid- or gas-phase applications. Over the past decade, the development of MOF/fiber composites fabrication strategies has encouraged further investigations into their potential applications for toxic gas adsorption,^{41,42} water purification,^{40,43} catalytic degradation of chemical warfare agents,^{13,34,38,46,47,54,62,67} and biomedical applications.⁴⁸

Several limitations exist in the previously reported strategies for the production of MOF/fiber composites that ultimately impede their widespread application. Textile fiber surfaces are typically chemically inert and disadvantageous for MOF nucleation and growth during coating synthesis. For example, the most widely used solvothermal method demonstrated a very low efficiency in coating MOF on fiber, yielding 5 to 20 times more free MOF particles in the reaction media as compared to the amount coated onto the fibers' surfaces.⁵² Chemically modifying the textile support with reactive groups (carboxylates, amines, hydroxyls, etc.) that mimic MOF linker and node functionalities promotes MOF nucleation on the fiber.⁴⁸ Alternatively, the deposition of a reactive template, namely a metal oxide (ZnO, Al₂O₃, etc.), onto a support generates seeding sites for linker coordination and allows for MOF nucleation. Of such deposition strategies, atomic layer deposition (ALD) affords a homogeneous metal oxide layer, which in turn facilitates a controlled, uniform MOF coverage on the support.^{51,52}

Through support functionalization, the expanded library of textiles offers a variety of possible fiber candidates for a composite, depending on a specific application. However, commonly used solvothermal syntheses can degrade thermally sensitive fibrous substrates. MOFs require high temperature synthetic conditions, often exceeding 100 °C, in hazardous organic solvents such as dimethylformamide (DMF), diethylformamide (DEF), and dimethyl sulfoxide (DMSO). These demanding conditions preclude the integration of MOF

coatings onto polymeric fiber materials, many of which lack stability in hot organic solvents. For example, polyacrylonitrile (PAN), a widely used synthetic fiber, dissolves in DMF under MOF synthesis conditions. Although alternative coating routes, such as electrospinning, can circumvent these roadblocks to yield such MOF/synthetic fiber composites, the solvothermal methods generally utilize inexpensive equipment, as compared to electrospinning.⁴¹ During the coating synthesis, MOF pores often trap hazardous solvents, such as DMSO and DMF, and pose a potential risk if the composites are used in human protection gear. Moreover, the synthesis of bulk MOF/fiber composites using high temperatures and highly flammable organic solvents presents significant safety concerns within industrial settings. Thus, MOF/fiber composite synthesis methods under more industrially relevant temperatures and in an environmentally friendly solvent, such as water, are desired to lower the cost of production and minimize the environmental impacts.

The aim of this review is to provide a focused overview of the most recently published studies regarding the fabrication and application of MOF/fiber composites. We also point out the existing problems associated with different production methods, as well as our perspective on future directions and studies.

2. SYNTHESIS METHODS OF MOF/FIBER COMPOSITES

2.1. *In Situ* Coating MOFs on Fiber Surfaces. 2.1.1. *Direct Solvothermal Growth.* Kùsgens's group, among other research teams, pioneered seminal work on the direct, *in situ* coating of MOFs on a fibrous substrate.³⁶ Several kraft pulp fibers and paper sheets supported HKUST-1 growth through a direct solvothermal synthesis method. The addition of the fibers to the HKUST-1 precursor solution under heating resulted in the growth of MOF particles on the substrate. The authors observed that the pulp fibers with higher lignin content contained greater HKUST-1 loading. The carboxylic groups found on lignin

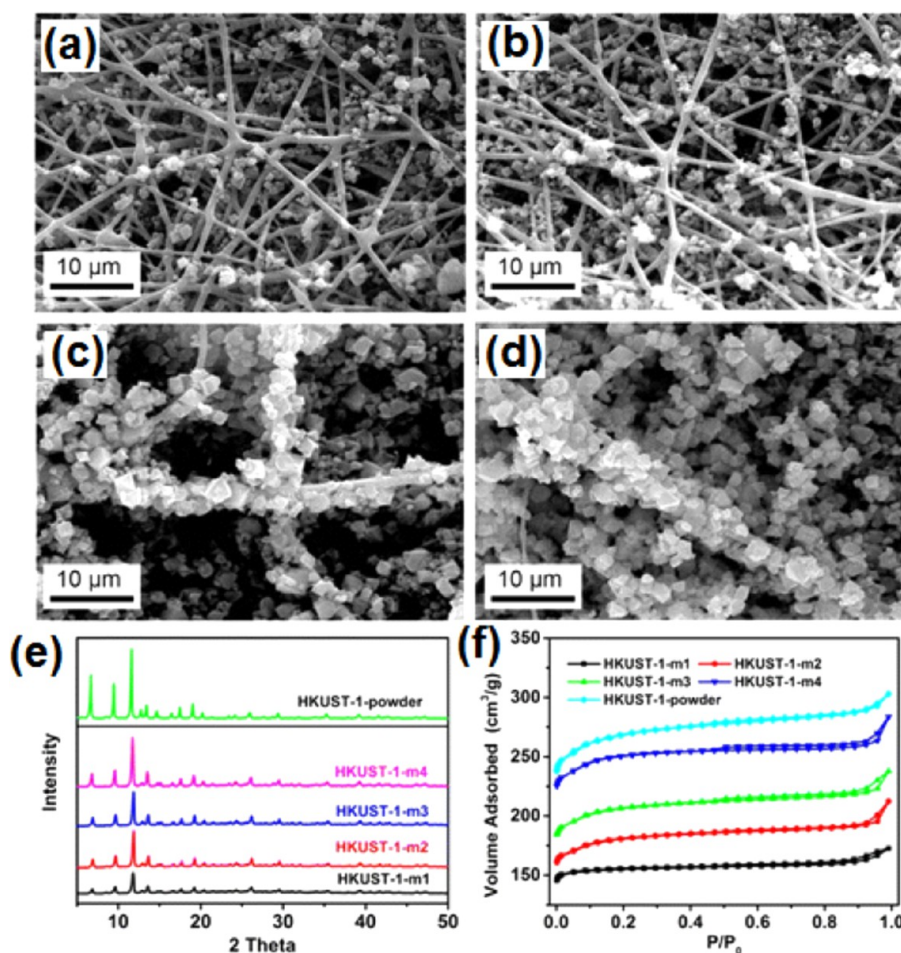


Figure 2. SEM images of HKUST-1 coated nanofiber after (a) one, (b) two, (c) three, and (d) four synthesis cycles. (e) PXRD patterns and (f) N_2 sorption isotherms of HKUST-1/nanofiber composites after different growth cycles. Adapted with permission from ref 37. Copyright 2016 American Chemical Society.

mimic those of the benzenetricarboxylate linker of the MOF, which enabled the higher MOF loading. However, inconsistent lignin amounts on the fiber resulted in nonuniform coverage of the coating on the pulp fiber surface. SEM images revealed loosely bonded HKUST-1 particles on fiber surface, implying the poor stability of the coating. In the direct solvothermal synthesis, most of the MOF nucleation occurs in the solvent rather than on the fiber surface, thus wasting reactants. Therefore, the direct solvothermal methods limit the resulting MOF mass loading on the fiber.

To increase MOF loading on the fibrous substrates, Liu et al. added electrospun nanofiber substrates, composed of poly(acrylic acid), poly(vinyl alcohol), and SiO_2 , into a precursor solution, which then supported four different MOFs.³⁷ A common solvothermal coating method deposited HKUST-1 and MIL-53(Al) onto fiber substrates, while a microwave-assisted solvothermal synthesis incorporated ZIF-8 and MIL-88B(Fe). Despite the functional groups ($-OH$ and $-COOH$) present on the fiber surface, the authors obtained a coating with nominal MOF growth after one cycle of the solvothermal synthesis. To improve the mass loading, repetition of the solvothermal synthesis procedure yielded composite samples labeled as HKUST-1-m1, HKUST-1-m2, HKUST-1-m3, and HKUST-1-m4, corresponding to one through four respective synthetic cycles (Figure 2). The intensity of powder X-ray diffraction (PXRD) patterns consistent with HKUST-1 increased with the repetition of the growth cycles due to more MOF crystals on the fiber surface, consistent with SEM imaging. The N_2 sorption isotherms exhibited an increase in the composites' porosity correspondingly with the increasing cycles.

By fine-tuning the reaction conditions, our team developed an environmentally friendly template-free aqueous synthesis strategy to

coat zirconium MOFs, including MOF-808 and $UiO-66-NH_2$, onto textile fiber.³⁸ We discovered the critical role of trifluoroacetic acid (TFA) as a modulator in the synthesis to yield a uniform coating morphology on a fiber surface. As a direct result of using TFA, the MOF crystallization only occurred on the fibrous support rather than as a free-flowing powder suspended in solvent. Interestingly, when we replaced TFA with other organic acids such as acetic acid and formic acid, most of the MOF particles instead formed in the reaction media, resulting in a nonuniform MOF coating on the fiber surface. From a combination of SEM, PXRD, and N_2 sorption studies during the template-free synthesis, our team proposed a three-stage mechanism: (1) formation of an amorphous coordination polymer on the fiber surface to template MOF growth, (2) generation of MOF nuclei, and (3) growth into a continuous MOF coating with high coverage (Figure 3). We demonstrated the first strategy to accomplish a MOF coating synthesis in an aqueous system, which offers a strategy to achieve polymeric fiber/MOF composites as most polymeric fibers lack stability in polar organic solvents like DMF. Moreover, our versatile methodology also formed MOF/fiber composites with PET, PP, and polyimide (PI), scalable to 1 m for coating MOF-808 on PET.³⁸

2.1.2. Biomineralization Inspired Synthesis. Biomineralization describes the process of generating biomineral shells and skeleton tissues; biomolecules not only accelerate the mineralization process of the inorganic materials but also supply an anchoring surface for the biomineral to form robust biomolecule–mineral composites. Inspired by biomineralization, Li et al. prepared MOF/fiber composites based on electrospun silk nanofibers (ESFs) as the biomacromolecule substrate and two zeolitic imidazole frameworks (ZIF-8 and ZIF-67) as coatings.⁴⁰ The silk nanofiber substrates were immersed in precursor

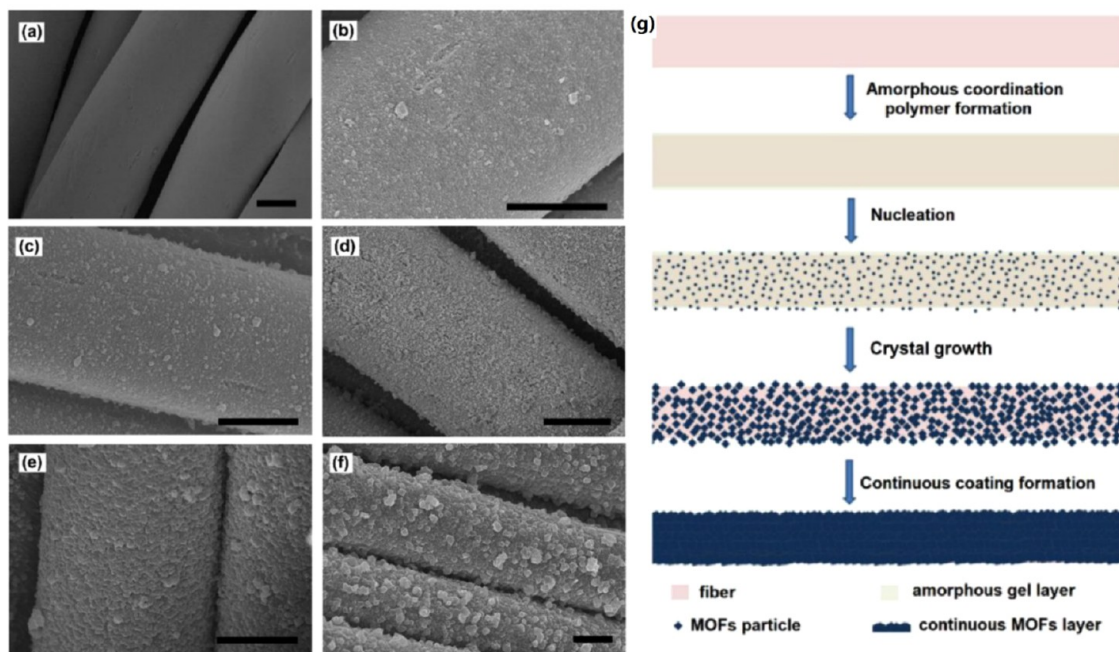


Figure 3. SEM images demonstrating the change in the fiber surface during the template-free aqueous synthesis of the MOF-808 coating. (a) PET fiber, after reaction time of (b) 10 min, (c) 20 min, (d) 30 min, (e) 60 min, and (f) 120 min. Scale bars: 5 μm . (g) Schematic illustration of template-free aqueous synthesis of Zr-MOF coating on fiber. Adapted with permission from ref 38. Copyright 2019 American Chemical Society.

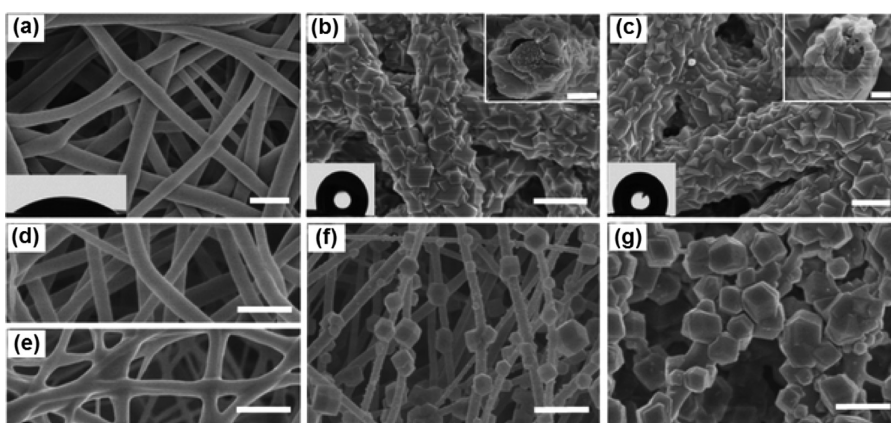


Figure 4. SEM images of ESF. (a) ZIF-8/ESF with the sectional section view the top inset, (b) ZIF-67/ESF with the sectional view in the top inset, (c) PAN nanofiber, (d) PU nanofiber, (d) ZIF-8/PAN, (f and g) ZIF-8/PU composite. Adapted with permission from ref 40. Copyright 2018 The Royal Society of Chemistry.

mixtures and then incubated at 38 $^{\circ}\text{C}$ for the ZIF-8 coating and 80 $^{\circ}\text{C}$ for ZIF-67 for 1 h. In both cases, the silk nanofiber composites displayed densely covered crystalline coatings (Figure 4a–c), which was also confirmed by PXRD as the targeted ZIFs' structures. SEM images of sectional views demonstrated a core–shell structure. Interestingly, the MOF coating revealed a clear intergrown morphology, which implied improved stability and higher loading of the coating. The authors also compared two synthetic polymer nanofiber substrates, polyacrylonitrile (PAN) and polyurethane (PU), in the deposition of the MOF layer. However, fabrication on the synthetic polymer substrates resulted in loose coating structures on the fibers with poor uniformity (Figure 4d–g), highlighting the importance of the chemical structure of silk biosubstrates in inducing MOF nucleation and growth.

2.1.3. Atomic Layer Deposited Metal Oxide Directed Growth. From the works studying MOF film formation on inorganic substrates, researchers identified precursors that could react with inorganic substrates to form a MOF nucleation layer.³² Parsons and team developed a general method to fabricate MOF/fiber composites, in which a metal oxide (ZnO, Al_2O_3 , and TiO_2) nucleation layer was

deposited on polymeric fiber surface via atomic layer deposition (ALD) to facilitate the MOF nucleation and growth.^{36,39,52,60} The authors observed that the ALD alumina thin layer deposited on polypropylene (PP) fibers enabled conformal growth of dense HKUST-1 coating on the fiber surface using solvothermal synthesis as shown in Figure 5.³⁹ Compared to the untreated PP fibers, the HKUST-1 areal loading increased from 9.61 mg/cm^2 to 14.78 mg/cm^2 with the ALD Al_2O_3 nucleation layer, to achieve one of the highest reported MOF mass loadings (75.3%) on fiber. Additionally, other fiber substrates, including polybutylene terephthalate (PBT) and cotton fibers, and other MOFs, such as MOF-74 and UiO-66, formed composites with this generalizable strategy. The study also explored the growth mechanism of HKUST-1 growth on different ALD metal oxides, including ZnO, Al_2O_3 , and TiO_2 , in the solvothermal synthesis.^{43,60} Of these oxides, the ALD ZnO deposited fiber facilitated the fastest growth. PXRD studies revealed that the ZnO template layer exhibited higher reactivity with the $\text{Cu}(\text{NO}_3)_2$ precursor to form a (Zn, Cu) hydroxy double salt intermediate, which undergoes a fast anion exchange with the ligand to form HKUST-1.

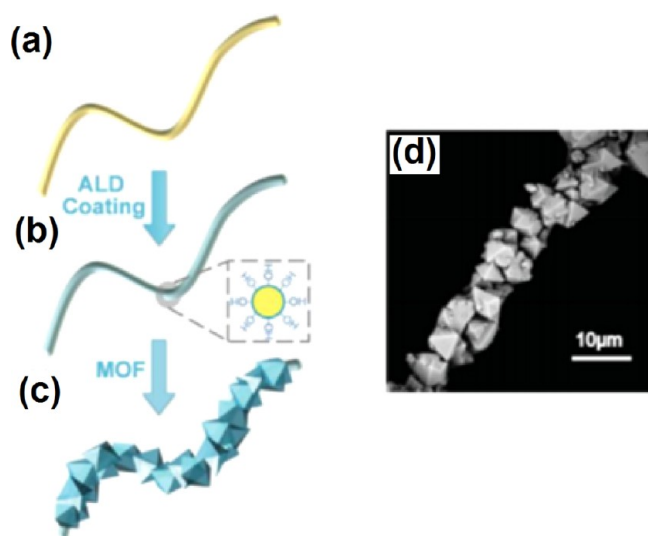


Figure 5. (a–c) Illustration of ALD metal oxide directed thermal growth of MOF coating on fiber surface. (d) SEM image of HKUST-1 coating on ALD alumina deposited PP fiber. Adapted with permission from ref 39. Copyright 2014 The Royal Society of Chemistry.

The team also deposited a TiO_2 ALD nucleation layer (5 nm) onto electrospun PA-6 nanofiber, and a solvothermal synthesis incorporated Zr-MOF on the TiO_2 coated PA-6 nanofibers (denoted as PA-6@ TiO_2 in this work).⁵¹ SEM and TEM imaging revealed dense MOF coatings on the nanofiber surface for all three types of Zr-based UiO-type MOFs, including UiO-66, UiO-66-NH₂, and UiO-67 (Figure 6).⁵¹ PXRD and N₂ isotherms indicated respective high crystallinity and porosity of the Zr-MOF coating on the nanofibers. Conformal morphology of the incorporated MOF improved the robustness of the coating, which maintained its structural integrity even after catalytic applications. In a comparison study, the MOF coating obtained on PA-6 without TiO_2 deposition featured poor coverage and aggregation. The mechanism study illustrated a difference in the role of the ALD TiO_2 layer in Zr-MOF deposition as compared to the HKUST-1 coating. The ALD TiO_2 layer acted as a nucleation layer for ligand attachment, rather than forming the intermediate via the reaction with the zirconium salt. Similarly, they also coated UiO-66-NH₂ MOF onto an inexpensive and readily available PP nonwoven textile using the straightforward method.⁵²

2.1.4. Layer-by-Layer Growth Method. Similar to a direct solvothermal synthesis, a layer-by-layer (LbL) growth approach promotes MOF growth on fiber substrates possessing functional groups, such as $-\text{COOH}$ and $-\text{NH}_2$. Morsali and co-workers investigated an ultrasound treatment assisted LbL method to grow HKUST-1 and MOF-5 on a silk fiber surface.^{35,61} The silk substrates

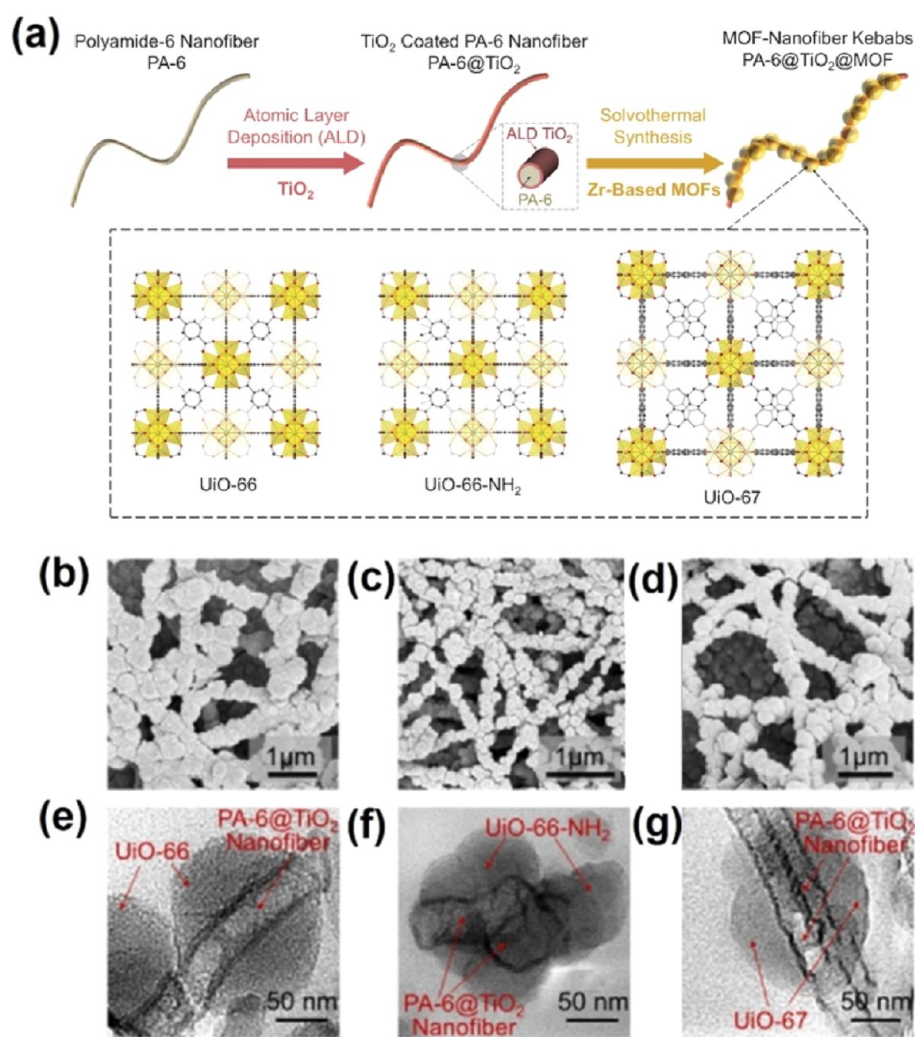


Figure 6. (a) Illustration of the ALD TiO_2 directed growth of Zr-MOF on PA-6 nanofiber substrates. SEM and TEM images of (b, e) UiO-66 coating on PA@ TiO_2 nanofibers, (c, f) UiO-66-NH₂ coating on PA@ TiO_2 nanofibers, and (f, g) UiO-67 coating on PA@ TiO_2 nanofibers. Adapted with permission from ref 51. Copyright 2016 John Wiley and Sons.

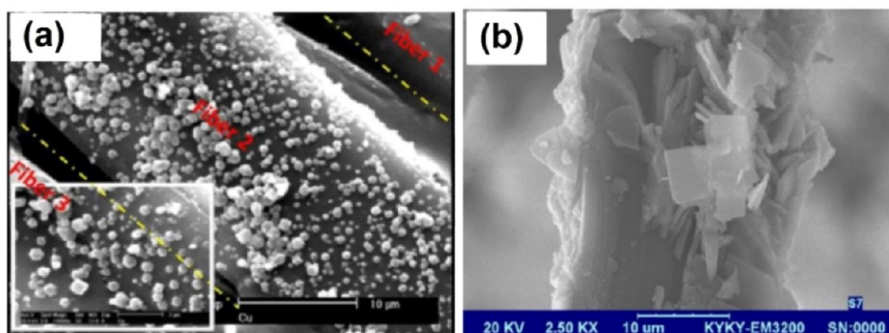


Figure 7. SEM images of (a) HKUST-1 and (b) MOF-5 coated silk fibers formed using a direct LbL growth method. Panel a: Adapted with permission from ref 35. Copyright 2012 Elsevier. Panel b: Adapted with permission from ref 61. Copyright 2014 Elsevier.

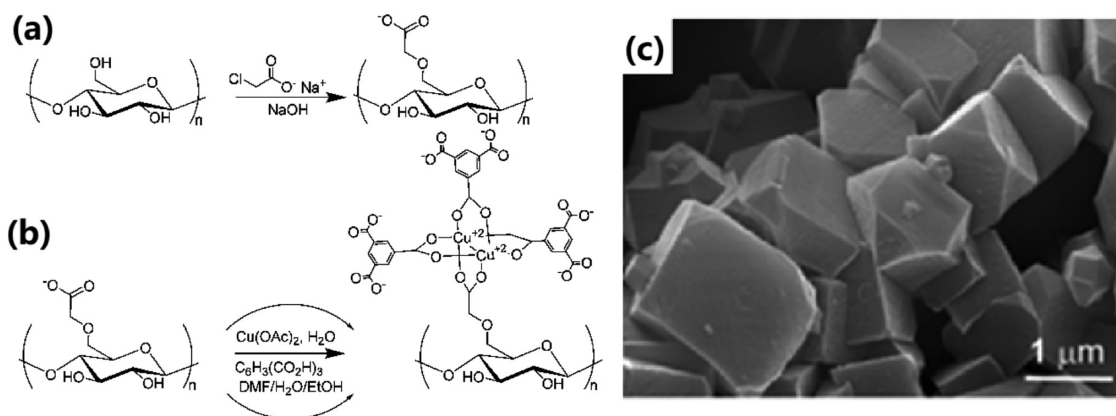


Figure 8. (a) Scheme for the grafting of carboxymethyl groups onto cellulose and (b) a proposed mechanism for HKUST-1 LbL growth on cellulose fiber. (c) SEM image of HKUST-1 coated cotton fibers. Adapted with permission from ref 48. Copyright 2015 American Chemical Society.

were sequentially dipped into a metal salt solution and organic ligand solution, followed by washing steps to remove any unreacted precursors. Sonication treatment accelerated the LbL growth reaction and improved the uniformity of MOF coatings on the silk fibers in both cases. However, this method precluded the synthesis of MOF/silk composite coatings with a high mass loading and full coverage (Figure 7). The lack or low density of functional groups on the untreated fiber surface prevented favorable metal ion/organic linker anchoring events for MOF nucleation during the LbL process and likely accounted for the poor coverage.

To improve MOF nucleation on surfaces, Biemmi et al. developed a chemical modification assisted growth method to coat oriented MOFs onto hard surfaces, such as gold.³³ This work demonstrated a robust and general strategy for nanoparticle coating and patterning. In this approach, self-assembled monolayers (SAM) of 11-mercaptoundecanoic acid and the complex ligand 11-mercaptoundecanol were grafted onto a substrate, where they acted as linkers. Following this, metal ions chemically adsorbed onto the SAMs as a starting layer for reacting with specific linker to form MOF coatings.

Extending the work developed by Biemmi, Neufeld et al. reported a method to coat HKUST-1 on cotton cellulose fibers using the LbL method.⁴⁸ Carboxylate groups were first grafted onto cotton cellulose, which supplied coordination sites for the copper ions and facilitated HKUST-1 growth as illustrated in Figure 8a. During eight LbL cycles, the cotton fiber soaked in an aqueous copper salt solution and then the BTCA ligand in DMF/ethanol/water (1:1:1) solution. As a result, a dense HKUST-1 coating formed as verified through SEM imaging of the fiber surface and PXRD studies of the resulting crystalline composite (Figure 8c). Results from these two highlighted LbL studies demonstrate that the preliminary functionalization of the desired substrate can circumvent low MOF composite coatings, thereby increasing the number of coordination sites for MOF growth.

The efficacy of ALD deposited metal oxide layers as nucleation sites for direct MOF solvothermal coating on fiber surfaces as well as MOF

synthesis mediated through LbL prompted the combination of the strategies to achieve MOF growth with a controlled thickness.⁴² Zhao et al. studied the ultrasound assisted growth of HKUST-1 coating on ALD- Al_2O_3 deposited polypropylene (PP) fibers, as described in Figure 9. As determined through SEM and TEM imaging, the 40 LbL growth cycles achieved a conformal and uniform HKUST-1 coating without noticeable agglomeration of HKUST-1 crystals in the voids between fibers (Figure 9b–e). Thus, the authors observed that LbL growth cycles dictated MOF film thickness and mass loadings, illustrating the tunability this method affords. However, the mass loading for each growth cycle is relatively low, inconvenient for yielding dense coatings on fiber. This synthetic method achieved the coating of a HKUST-1 layer on both polyethylene terephthalate and cotton fiber substrates to highlight its generality.

2.1.5. Coordination Replication from Solid Precursor. Another method emerged that capitalized on the coordination replication directly from a cheap, insoluble precursor to prepare MOF/fiber composites. Kitagawa and co-workers developed the technique as shown in Figure 10a,b.³² The authors achieved the morphologic replacement of a shaped sacrificial metal oxide (Al_2O_3), acting as both a metal ion source and an “architecture-directing agent,” to yield a well-structured MOF architecture. This pseudomorphic replication approach obtained Al-MOF based 1D nanofibers in addition to the 2D and 3D mesoscopic architectures.^{32,56} To form the precursor template, a facile solution-processed method was used to prepare alumina nanofibers for 1-D Al-MOF nanofiber synthesis.⁵⁶ This differed for 2D and 3D precursor structures, which employed a polymeric bead templated method for precursor preparation.³²

The team proposed a coupled “dissolution–reprecipitation” mechanism for the explanation of liquid–solid interfacial reaction. Initially, the dissolved precursor forms an interface layer filled with aluminum ions. Followed by a fast coordination reaction between dissolved cations and ligands, a MOF forms on the substrate’s surface. With the consumption of the metal ion, the interface layer regenerates

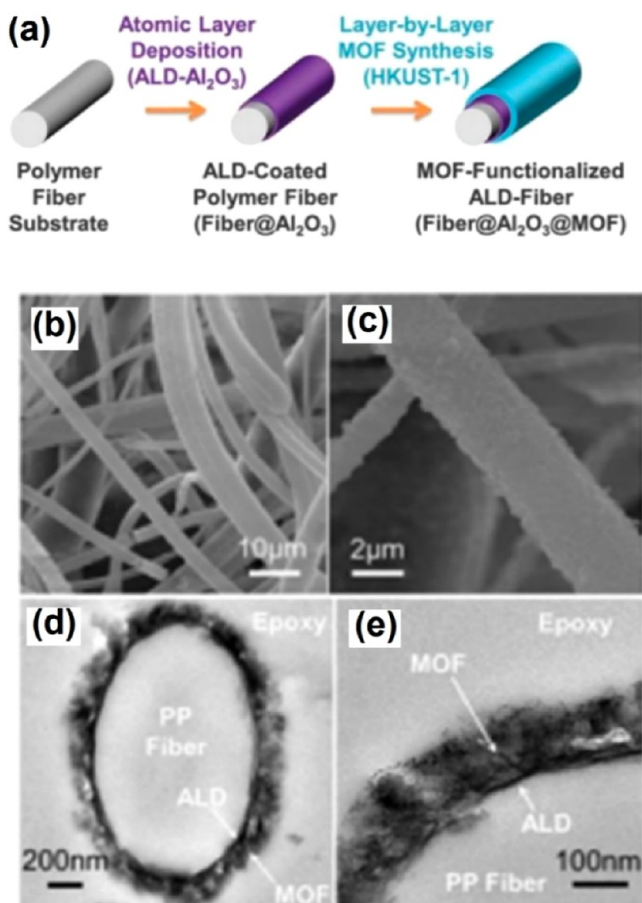


Figure 9. (a) Illustration of the LbL synthesis of HKUST-1 coating using ALD-Al₂O₃ as the nucleation layer. (b,c) SEM images of prepared HKUST-1 coating on ALD-Al₂O₃ modified polypropylene (PP) fibers. (d,e) TEM images showing the cross-sectional view of HKUST-1 coating on ALD-Al₂O₃ modified PP fibers. Adapted with permission from ref 42. Copyright 2015 The Royal Society of Chemistry.

with freshly released metal ions to feed the MOF crystal growth in tandem with the predissolved organic ligand (Figure 10a). Contrasting with the slow kinetics of oxide dissolution, fast MOF crystallization kinetics result in a localized supersaturated metal ion layer only at the interface between the substrate surface and the ligand solution (Figure 10b). Hence MOF crystals continuously form only at the solid/liquid interface, provided a sufficient supply of precursors. On the basis of this mechanism, the authors incorporated aluminum MOFs, [Al(OH)(bdc)]_n and [Al(OH)(ndc)]_n, onto alumina nanofibers. As shown in Figure 10c, electrospinning Al(NO₃)₃ introduced the precursor to poly(methylglutarimide) (PMGI) nanofibers, which then formed self-standing alumina nanofibers after calcination treatment. The obtained alumina nanofiber substrate underwent heating at 180 °C for 1 min under microwave irradiation in a water solution of H₂ndc or H₂bdc to generate the corresponding Al-MOF with ~10% conversion from the alumina precursor (Figure 10d).⁵⁶ However, the overall composite demonstrated high fragility and poor processability because unreacted alumina nanofiber substrates supported the MOF layer, hindering its further application.

To build upon Kitagawa's seminal work, Parsons and co-workers synthesized a series of MOF/fiber composites via the coordination replication method using ALD deposited metal oxide on a fiber surface. Following the deposition of an alumina layer onto PP fiber, the textile was heated in a porphyrin linker solution [5,10,15,20-tetrakis(4-carboxyphenyl)porphyrin (TCPP)] to obtain an aluminum porphyrin framework coating directly on the fiber surface.⁵⁸ Rather than serving as an initial precursor, the ALD oxide layers functioned as a reactive template for the deposition of a desired metal precursor layer. For

example, ALD deposited ZnO on the fiber surface reacted with copper salt to form an intermediate (Zn, Cu) hydroxy double salt (HDS) solid layer. Following the formation of this layer on the fiber, exposure of the templated textile to a TCPP linker solution yielded the copper porphyrin framework (Cu-TCPP).⁵⁷ To improve MOF coverage on the fibers, Bechelany et al. investigated the effect of microwave-assisted heating procedures utilized in conjunction with coordination replication. The authors reported the synthesis of ZIF-8 and MIL-53-NH₂(Al) coatings on PAN nanofibers relying on ALD deposited zinc oxide or alumina.⁴⁴ Microwave-assisted heating of the ALD treated fibers at 100 °C in 2-methylimidazole and 2-aminoterephthalic acid solution yielded composites with increased and more uniform MOF coverage. When instead employing conventional heating for MOF formation, the resulting coating contained poor uniformity and coverage. Thus, microwave-assisted heating emerged as a powerful costrategy to access improved MOF/fiber composites.

The above ALD deposited solid layer served as a useful precursor for the synthesis of MOF coatings. In order to simplify the coordination replication process, the Xin team developed an inexpensive and scalable method to coat metal solid layers onto the fiber surface using an altered form of the coordination replication synthesis.⁵⁹ The precursor layer formed on the fiber surface through a facile solid-liquid interfacial reaction between potassium carbonate (K₂CO₃) impregnated in the fibers and the metal salt solution. An insoluble layered hydroxide salt (LHS), such as copper hydroxide nitrate (CHN), assembled on the fiber surface, acting as both the metal precursor and the template for MOF nucleation. Following immersion of the precursor solid-coated fiber in the organic ligand solution, the coordination replication reaction occurred at the interface between the solid layer and the solution. As a result, the process yielded a precise MOF coating composed of intergrown crystals on the fiber substrate as shown in Figure 11. This versatility incorporated four different MOFs (HKUST1, Cu-BDC, ZIF-8, and ZIF-67) onto a series of fibers (cotton fiber, commercial microfibers, and electrospun polyacrylonitrile nanofibers). The room temperature reaction conditions simplified scale-up efforts, and our teams produced a 1-*m* scale MOF-fabric composite.

2.1.6. Solvent-Free Hot-Pressing Method. Beyond solvothermal syntheses, Wang and co-workers presented a solvent-free approach for producing stable MOF coatings through a hot-pressing method, as illustrated in Figure 12a.^{45,63-65} For this method, an electric iron applied simultaneous high temperature and pressure to facilitate the rapid deposition of MOF layers onto various fibrous substrates (such as a carbon fiber or metal grid). As demonstrated in Figure 12b, two proposed reaction steps likely occur during the hot-press process. First, under heating and pressure, MOF precursors undergo chemical immobilization on the available sites of the substrate's surface. Then, MOF nucleation and crystal growth occur on the surface to form a stable coating.⁶⁵ The polymeric compound polyethylene glycol served as a surfactant in this method to promote the diffusion of the precursors. After synthesis, washing the MOF layers removed this surfactant. This strategy accomplished the synthesis of a variety of MOFs including carboxylate-based (MOF-5), imidazolate-based (ZIF-8), and mixed-metal MOF on various fiber substrates, such as carbon cloth, melamine sponge, glass fiber, and plastic mesh. Within the same study, layer-by-layer pressing also provided a strategy to generate superhydrophobic "Janus" MOF films that were traditionally water instable. Interestingly, this hot-press method increased the mechanical stability of the MOF coating as observed in abrasion resistance and stirring tests. X-ray photoelectron spectroscopy (XPS) analysis revealed a strong interaction between the MOF layer and fiber substrates. Importantly, this hot-pressing method can be scaled up through a continuous roll-to-roll production, an eco-friendly method that produces less toxic chemicals.⁶⁴ However, the high temperature (200 °C) and pressure may damage widely used polymeric fiber matrices, such as cotton, polyester, and nylon. However, this promising hot-pressing method must overcome limitations needed to be tackled, such as the undesired MOF aggregation on the fiber surface and the low mass gain for each hot-press cycle. Therefore, multiple coatings are necessary to get a high loading, which would be time-consuming in industrial production.

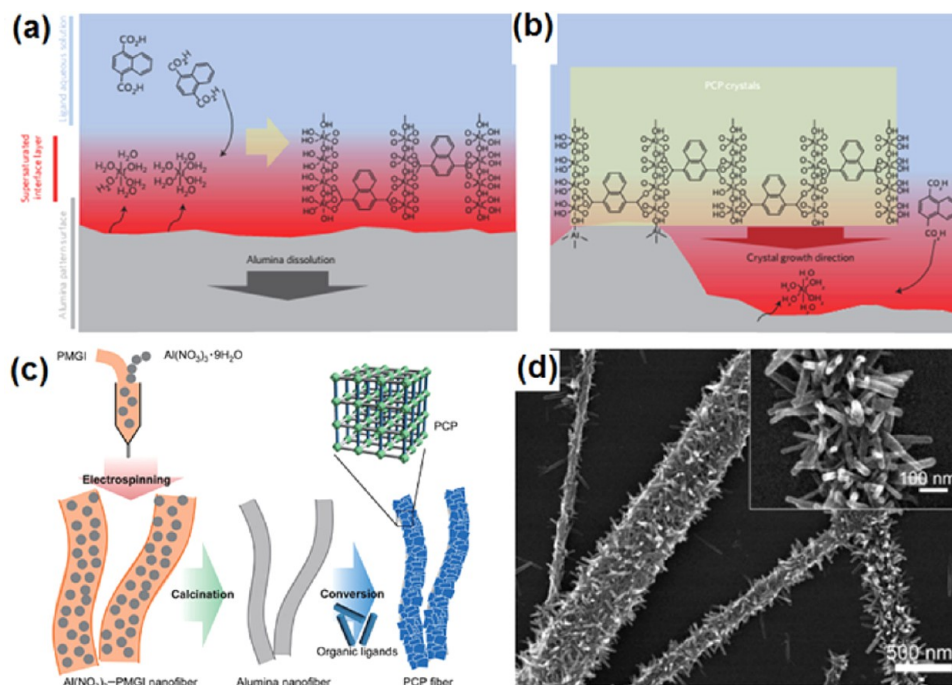


Figure 10. (a,b) Schematic illustration of the coordination replication mechanism proposed by Kitagawa and team. (c) Fabrication of aluminum MOF nanofiber by the coordination replication from alumina nanofiber precursor. (d) SEM image of $[\text{Al}(\text{OH})(\text{bdc})]_n/\text{alumina}$ nanofiber composite by coordination replication of solid precursor. Panels a and b: Adapted with permission from ref 32. Copyright 2012 Nature Publishing Group. Panels c and d: Adapted with permission from ref 56. Copyright 2014 The Chemical Society of Japan.

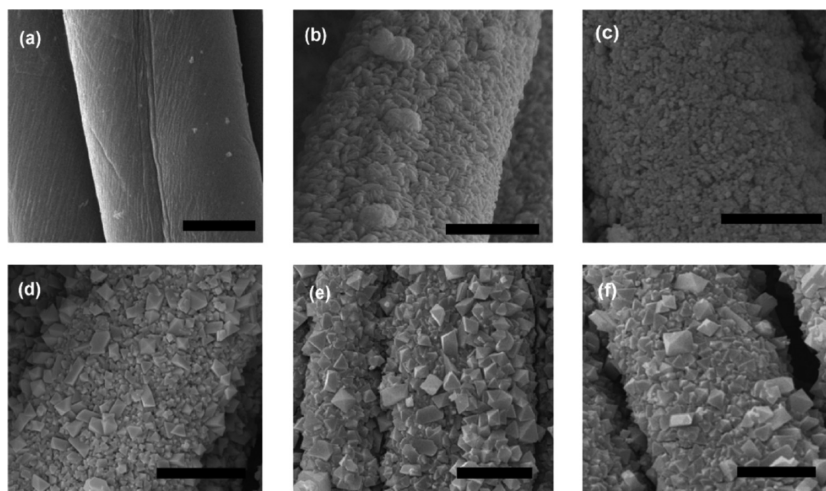


Figure 11. SEM images revealing the surface morphology evolution in the synthesis of HKUST-1 coating by coordination replication of CHN solid layer: (a) cotton fiber and (b) CHN-deposited cotton and after BTCA linker solution treatment for (c) 1, (d) 5, (e) 30, and (f) 60 min. All scale bars are $10\ \mu\text{m}$. Adapted with permission from ref 59. Copyright 2019 American Chemical Society.

Additionally, extension to other MOF families, such as zirconium-based and iron-based frameworks, can expand the targeted applications of this process.

2.1.7. Inkjet Printing Method. On the basis of the evaporation-induced crystallization mechanism,^{68,69} Zhuang et al. developed a direct printing strategy for positioning MOF coatings and patterns on flexible substrates.²⁹ Critical factors to consider within the inkjet printing process include the viscosity and surface tension of the precursor ink solution. Thus, the authors developed a printable ink formula employing ethylene glycol as a stabilizer for the precursors dissolved in an ethanol/DMSO solution. A commercial printer deposited the precursor ink onto a series of substrates, including a polyester film, office paper, and cotton fiber, to obtain MOF patterns after heat treatment (Figure 13). Adjusting the printing–drying cycles controlled

the thickness as well as the mass loading of the MOF layer. Given the relatively low yield of each printing cycle, the outlined method may be more attractive and suitable for processes requiring precise engineering.

2.2. Fabricating Composite from Presynthesized MOF.

2.2.1. Doping during Electrospinning. As highlighted in our prior section, electrospinning emerged as a facile and direct approach to fabricate MOF/fiber composites. The process spins the blended suspension of the MOF nanoparticles and polymers under a high voltage.^{41,46,47,55} The method enabled the use of polymer substrates normally miscible in polar organic solvents such as DMF. Many types of polymers, including PAN,^{41,53} PS,⁴¹ polyvinylpyrrolidone (PVP),^{41,53} and PVDF,^{38,47} served as substrates in the electrospinning method for the fabrication of MOF/nanofiber composite. Wang and co-workers illustrated the generalizability of this fabrication strategy for different

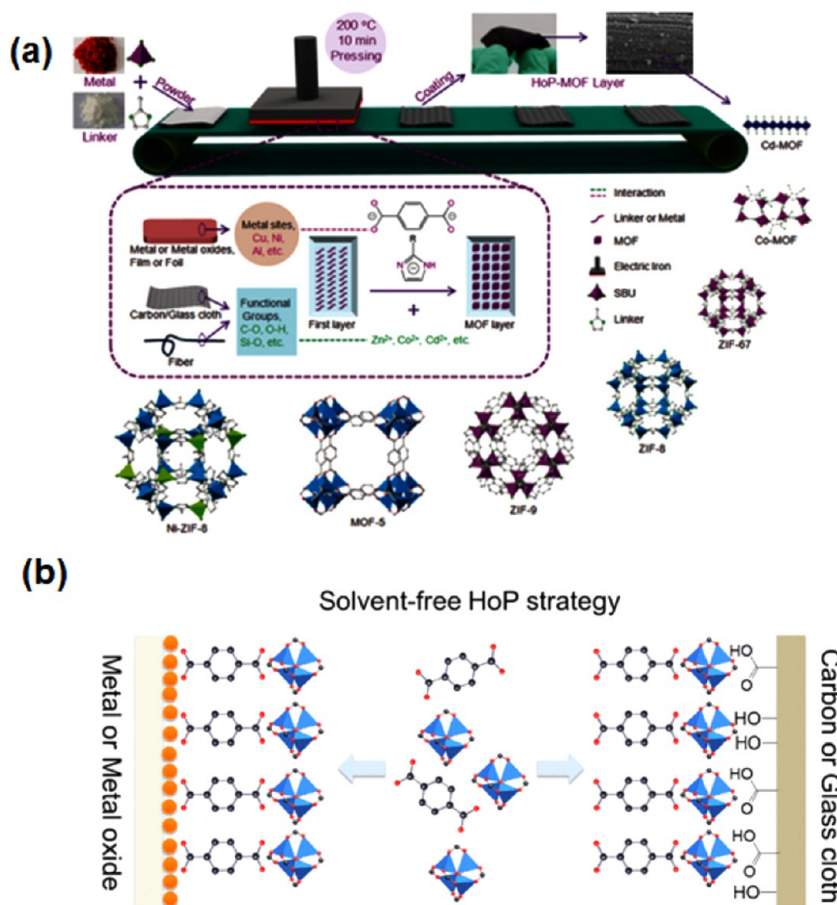


Figure 12. (a) Schematic representation of the solvent-free hot-pressing (HoP) strategy. (b) The proposed interaction mechanism between the precursors and fiber substrates during MOF deposition. Panel a: Adapted with permission from ref 45. Copyright 2016 John Wiley and Sons. Panel b: Adapted with permission from ref 65. Copyright 2019 American Chemical Society.

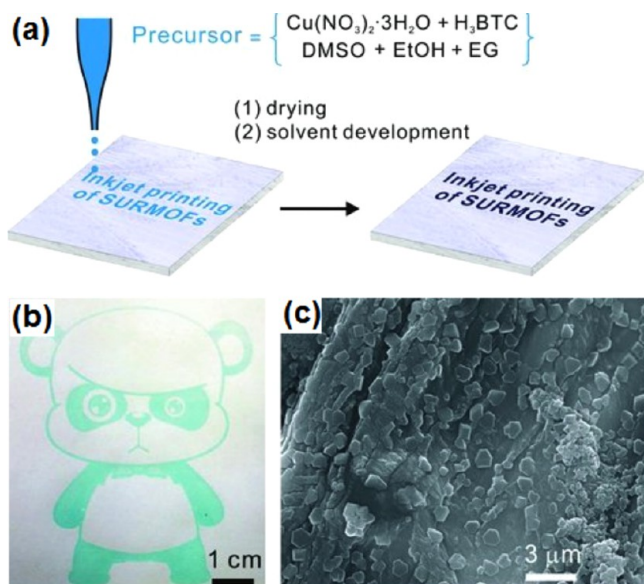


Figure 13. (a) Illustration of inkjet printing of HKUST-1 onto flexible substrates using a precursor solution as the ink. (b) Photograph image and (c) SEM image of a HKUST-1 pattern on office paper. Adapted with permission from ref 29. Copyright 2013 John Wiley and Sons.

polymer substrates, including PAN, PS, and PVP, supporting doped MOF nanoparticles (Figure 14).⁴¹ The method achieved very high

MOF mass loading (up to 60 wt %) and excellent MOF particle dispersion behavior. Importantly, MOF nanoparticles retained their porosity and surface area after their postsynthetic deposition onto the fiber. The composites remained highly flexible, but they demonstrated diminished structural integrity. To improve their robustness, the authors incorporated other supporting substrates, such as metal mesh or nonwoven fabric, to reinforce the structure of the MOF/nanofiber composite. Despite this structural improvement, the electrospun composites could not undergo applications in some media, such as DMF, due to the solubility of the polymer substrates in such polar solvents.

Additional work by López-Maya et al. enhanced the electrospinning process for postsynthetic deposition of MOFs onto fibers. The authors developed a process to introduce MOF nanoparticles onto silk nanofiber substrates by spray drying, an emerging method to dope nanofibers during electrospinning.⁴⁶ A UiO-66 suspension was sprayed over the silk nanofibers during the electrospinning process. The imbedded MOF nanoparticles in the void of silk nanofiber substrates formed a UiO-66/nanofiber composite material. Though this method achieved high MOF mass loading (above 60%) in the composite, weak interactions between the MOF nanoparticles and substrate led to an unstable composite. Leaching of the functional MOF nanoparticle reduced the viability of this fabrication method for industrial applications.

2.2.2. Postsynthetic Polymerization Method. To improve the dispersion and cohesion of MOF particles with a polymer substrate, postsynthetic polymerization (PSP) added binding sites on the MOF linker to react with polymer monomers and form covalent bonds around MOF particles.²⁷ Cohen and co-workers reported a simple yet powerful postsynthetic polymerization (PSP) method to fabricate a covalently bound MOF/nylon composite as shown in Figure 15a.⁵⁴

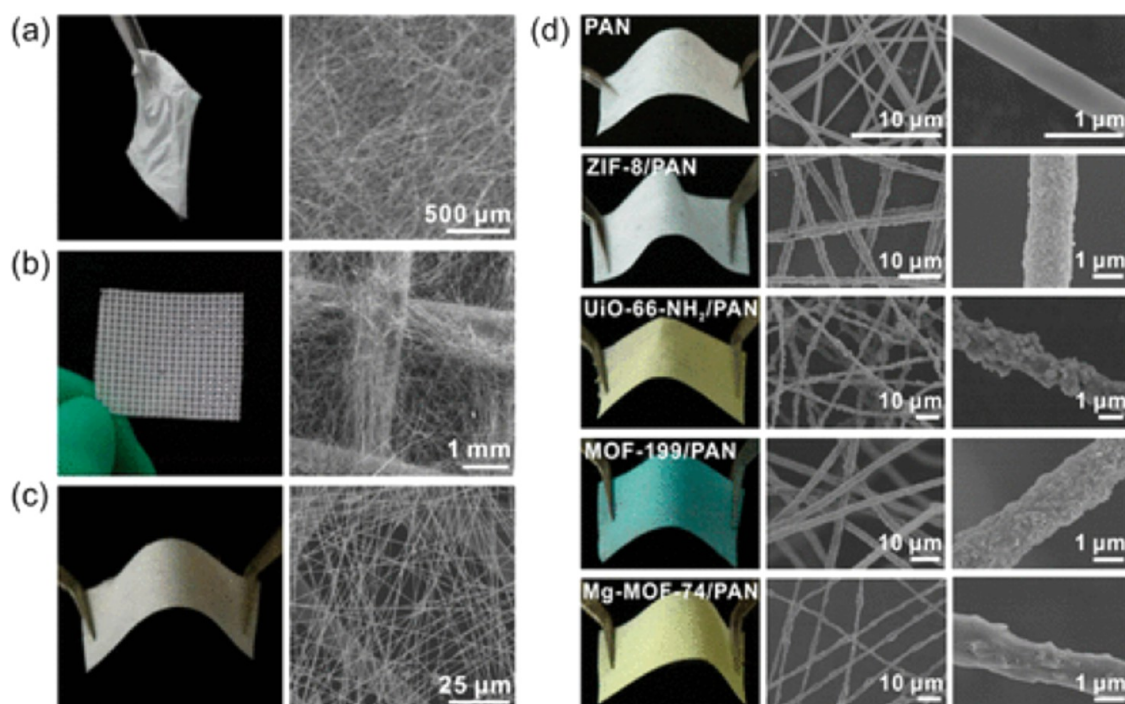


Figure 14. Photograph and SEM images of (a) free-standing ZIF-8/PAN nanofiber composite, (b) ZIF-8/PAN nanofiber composite supported on a metal mesh and (c) nonwoven textile. (d) Photographs and SEM images of MOF/PAN nanofiber composites supported on a nonwoven fabric piece. (Adapted with permission from ref 41. Copyright 2016 American Chemical Society.).

Postsynthetic modification (PSM) of UiO-66-NH₂ coupled the MOF to adipoyl chloride to introduce reactive acyl chloride groups on the ligands of MOF. The functionalized UiO-66-int (int: intermediate) and 10 equivalents of adipoyl chloride in ethyl acetate (EtOAc) was carefully poured over a water solution of hexamethylenediamine (HMDA). Copolymerization only occurred at the interface of the two phases, during which the UiO-66-int component covalently bonded to the PA-66 polymer chain. Simple stretching of the resulting PA-66-UiO-66-NH₂ further engineered the hybrid into a flexible fiber (Figure 15b). PXRD and SEM studies verified the introduction of the UiO-66-NH₂ MOF particles in the composite fiber (Figure 15c). The reaction of the modified UiO-66-NH₂ MOF component with the precursors of nylon polymer during the interfacial polymerization yielded a composite material with a MOF mass loading of about 29%. The covalently coupled UiO-66-NH₂/PA-66 fiber composite demonstrated nearly an order of magnitude improvement in the catalytic hydrolysis of a nerve agent simulant (dimethyl-4-nitrophenylphosphate, DMNP) compared to MOFs physically embedded in nylon substrates.

2.2.3. Covalent Immobilization Coating Method. Direct coating of preformed MOF particles on commercial fiber substrates could be more attractive for large-scale applications. Li and co-workers reported an eco-friendly coating method for the covalent immobilization of MIL-101(Cr) on nylon fiber by γ -ray initiated cograft polymerization with 2-hydroxyethyl acrylate (Figure 16a).⁴⁹ Briefly, the authors casted a mixture of 2-hydroxyethyl acrylate monomer and MIL-101(Cr) nanoparticles in ethanol onto the nylon fabric, and they irradiated the composite with a ⁶⁰Co γ -ray source at room temperature to initiate the copolymerization. The γ -ray irradiation generated free radicals on the nylon and MOF surfaces underneath, which promoted the graft polymerization with 2-hydroxyethyl acrylate to form a network of covalently tethered MIL-101 nanoparticles on fiber surface. SEM revealed MOF particles on the nylon fiber surface after the γ -ray radiation induced cograft polymerization, while PXRD indicated the intact crystalline structure of the MIL-101(Cr) particles. The MOF coating layer served as an efficient aromatic carrier for the textile and supplied the sustained release of organic aromatics encapsulated within the grafted MOFs. Following the MOF coating, the textile turned green (Figure 16b), which could serve as an advantageous alternative from the

conventional dyeing processes with high pollution. The MIL-101(Cr)/nylon composite exhibited excellent dry laundering durability. SEM and TGA (thermogravimetric analysis) confirmed that the MOF coating remained on the surface of the fiber even after 30 h of dry laundering (Figure 16c,d). Unfortunately, prolonged exposure to ⁶⁰Co γ -rays causes radiation damage and limits the scalability of this process.

2.2.4. Supramolecular Assembly. Lee et al. reported a facile composite fabrication to coat presynthesized UiO-66-NH₂ nanocrystals onto a nonwoven polypropylene (PP) textile (Figure 17a).⁵⁰ β -Cyclodextrin (β -CD) and cetyltrimethylammonium bromide (CTAB) perform as surfactant assembly agents to chemically direct the fabrication. A rapid self-assembly on the MOF nanocrystal surface promoted the MOF nanocrystals adhesion onto the fiber surface. Rapid assembly of the composite avoided agglomeration of the nanocrystals during the fabrication (Figure 17b–d). ALD metal oxide thin layers supplied a hydrophilic surface on the support that further improved assembly uniformity and MOF coverage, resulting in a UiO-66-NH₂ mass loading as high as 40 wt % and a BET surface area above 200 m²/g for the composite. The authors evaluated the adhesion stability of the assembled UiO-66-NH₂ nanocrystals on the textile surface through vigorously stirring the composites at 500 rpm for 1 day. Mass loading measurement demonstrated a loss of only 0.1% of the coating, indicating very strong bonding between MOF nanocrystals and the fiber surface. A brushing test on the UiO-66-NH₂/PP composite further investigated the MOF coating's mechanical stability. After 30 manual brushing cycles, the brush contained negligible MOF particles, and the original yellow color of the composite stayed intact. Thus, the strong adhesion of the MOF coating on the fiber surface prevented significant damage inflicted by the brushing force. While this method is powerful and straightforward, potential aggregation of MOF particles in the fiber void may hinder the diffusion or obstruct the accessibility of guest molecules into the MOF cavities. Therefore, improving the coating uniformity can prevent aggregation of MOF particles in the fiber voids and ultimately enhance the performance of MOF/fiber composite.

2.2.5. Dip Coating Method. The textile industry frequently employs dip coating as a facile and scalable technology. Recently, we extended this method to develop MOF/fiber composites.⁶⁷ For this technique, we dipped a textile substrate into a mixture of presynthesized MOF-808

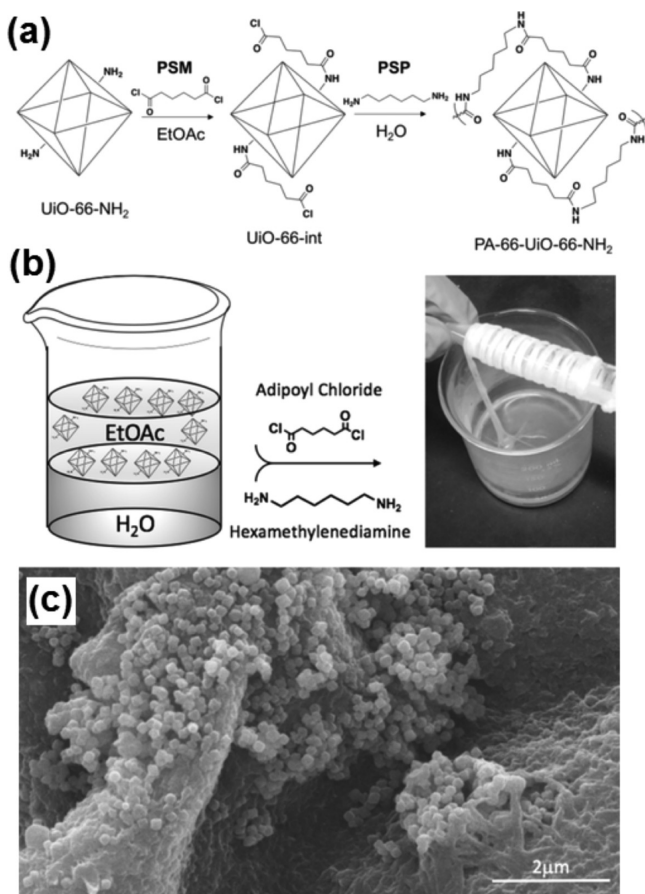


Figure 15. (a) Reaction route of the postsynthetic polymerization for introducing UiO-66-NH₂ into PA-66 polymer. (b) Illustration of interfacial fabrication method for UiO-66-NH₂/PA-66 fiber composite. (c) SEM image of UiO-66-NH₂/PA-66 fiber composite. Adapted with permission from ref 54. Copyright 2019 John Wiley and Sons.

nanoparticles and polyethylenimine (PEI) in methanol and dried it at room temperature to obtain a composited MOF-808/PEI coating with high coverage (Figure 18). The coating exhibited impressive stability when stirred in water at room temperature, owing to the low solubility of the PEI polymer that acted as a binder in the coating. Importantly, the installed PEI also performed the critical role of a potent base in the application of nerve agent catalytic hydrolysis. This straightforward strategy could allow for the introduction of different functionalities into MOF/fiber composites by adding the desired components (MOFs and polymers) in the coating stock. Furthermore, regular textile engineering equipment, such as roll-to-roll dip coating equipment, could scale up the approach. We envision this method will help advance MOF/fiber composites for large-scale, commercial productions.

3. APPLICATIONS OF MOF/FIBER COMPOSITES

3.1. Particulate Matter Removal. Particulate matter (PM), especially that with a diameter below 2.5 μm (PM_{2.5}), persists as a severe worldwide pollutant. Candidate solutions for the capture of PM include MOFs; unsaturated metal sites and defects within MOFs yield a charged surface, which could capture the highly polar PM through electrostatic interactions. Wang and co-workers explored the potential of MOF/filter composites for efficient PM capture as shown in Figure 19.⁴¹ They studied the PM filtration efficiency of their electrospun MOF/nanofiber composites under simulated conditions along with the real smog-filled atmosphere in Beijing. In this comparative study, they prepared four composites using

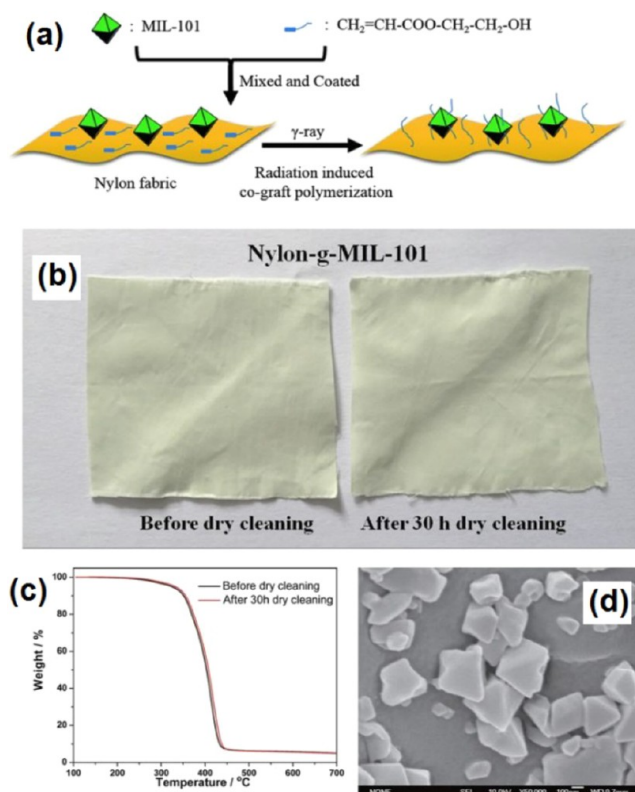


Figure 16. (a) Illustration of the fabrication of MOF/fiber composite by γ -ray initiated graft polymerization. (b) Photograph images of MIL-101/nylon composite before and after 30 h dry washing. (c) TGA curves of MIL-101/nylon composite before and after 30 h dry washing. (d) SEM image of MIL-101/nylon composite after 30 h dry washing. Adapted with permission from ref 49. Copyright 2016 Nature Publishing Group.

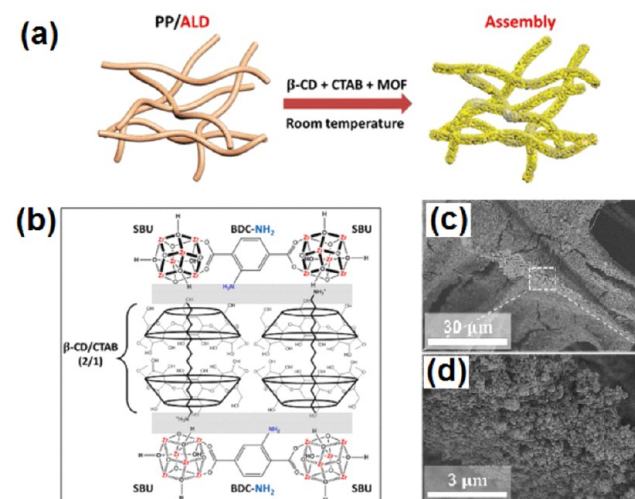


Figure 17. (a) Illustration of the supramolecular directed assembly strategy for UiO-66-NH₂/PP composite fabrication. (b) Schematic of expected interactions between MOF and the supramolecular complex (β -CD + CTAB). (c,d) SEM images of UiO-66-NH₂/PP composite by supramolecular directed assembly. Adapted with permission from ref 50. Copyright 2017 American Chemical Society.

polyacrylonitrile (PAN) as a polymeric substrate, while varying the functional MOF in the composite from MOF-199, UiO-66-NH₂, Mg-MOF-74, and ZIF-8. Under the real-world hazy

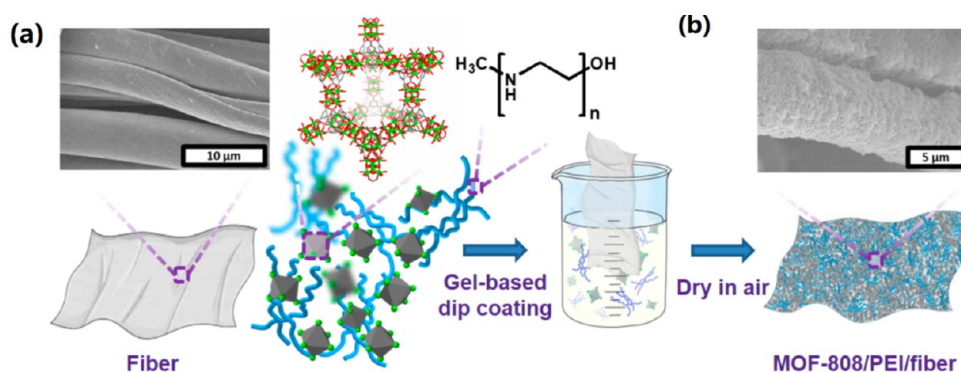


Figure 18. Schematic illustration of the dip coating method for the fabrication of a MOF-808/PEI/fiber composite. SEM images of (a) cotton fiber and (b) MOF-808/PEI/fiber. Adapted with permission from ref 67. Copyright 2019 American Chemical Society.

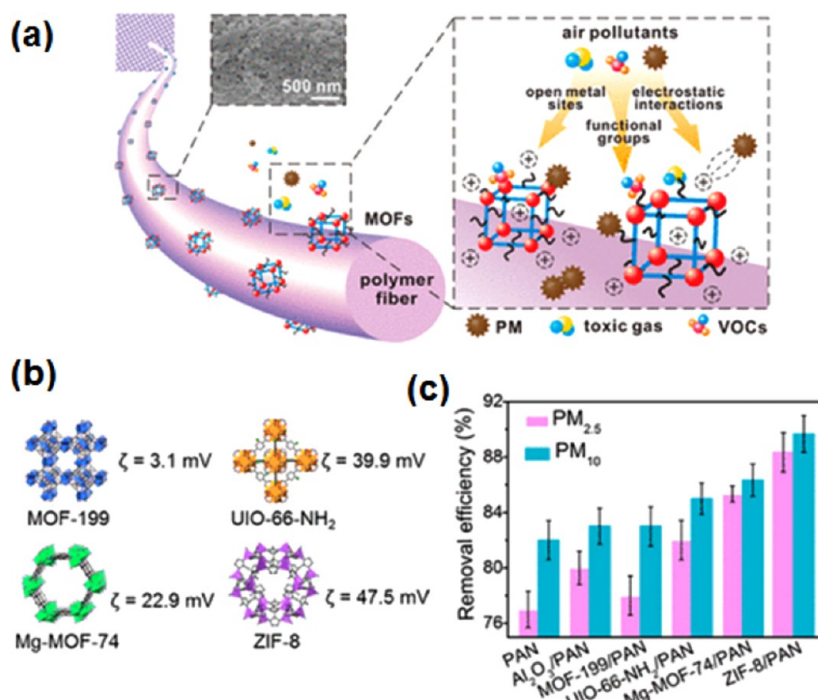


Figure 19. (a) Schematic depicting the removal mechanism of air pollutants using the MOF/fiber composite. (b) Zeta potentials (ζ) of MOFs used for nanofiber doping and (c) PM removal efficiency comparison using different nanofiber-based filters. Adapted with permission from ref 41. Copyright 2016 American Chemical Society.

conditions ($\text{PM}_{2.5}$, $350 \mu\text{g m}^{-3}$; PM_{10} , $720 \mu\text{g m}^{-3}$; relative humidity, 58.6%; and temperature, $23.5 \text{ }^\circ\text{C}$), their MOF/nanofiber composites all showed superior performance in PM removal compared to the pure PAN nanofiber. They observed positive correlations between the removal efficiency and zeta potential of the MOFs used in composites. For example, ZIF-8 contains the highest zeta potential value among the four MOFs, and its composites achieved the best performance in PM removal, with about 90% of the PM removed. The removal efficiency of ZIF-8/PAN nanofiber composite did not exhibit obvious degradation after a 48 h exposure in the previously mentioned hazy atmosphere. Additionally, it demonstrated an exceptionally high removal capacity of 29.5 g m^{-2} or 0.037 g g^{-1} .⁴¹ Similarly, MOF/fiber composites prepared using a roll-to-roll hot pressing method indicated excellent PM removal performance. Interestingly, the removal efficiency could be fully recovered after the sample underwent washing using tap water and subsequent drying.⁶⁴

3.2. Hazardous Gas Removal. Owing to the large amount of binding sites in MOFs for the adsorption of toxic industrial gases, such as NH_3 , SO_2 , HCl , and H_2S ,^{19–21} the incorporation of MOF/fiber composites into equipment can produce protective gear for these toxic species.^{30,39,41–43}

Parsons and co-workers investigated the NH_3 and H_2S removal performance of their HKUST-1/fiber composites, which were pre-coated with an ALD zinc oxide to facilitate the MOF growth.^{42,43} As previously mentioned in section 2.1.4, an LbL dipping method pretreated PP with an ALD zinc oxide layer to promote formation of the HKUST-1 coating layer. Increasing the number of LbL cycles improved the NH_3 adsorption capacities (Figure 20a,b). After 40 LbL cycles, the HKUST-1/PP composite with a mass loading of 17% exhibited an ammonia dynamic adsorption capacity of $1.37 \text{ mol NH}_3/\text{kg}$ composite (normalized as $7.63 \text{ mol NH}_3/\text{kg}$ MOF) and a H_2S dynamic loading of $1.49 \text{ mol H}_2\text{S}/\text{kg}$ composite (normalized as $9.46 \text{ mol H}_2\text{S}/\text{kg}$ MOF). They also prepared a HKUST-1 coating on PAN nanofibers and PP microfibers via a one-step synthesis

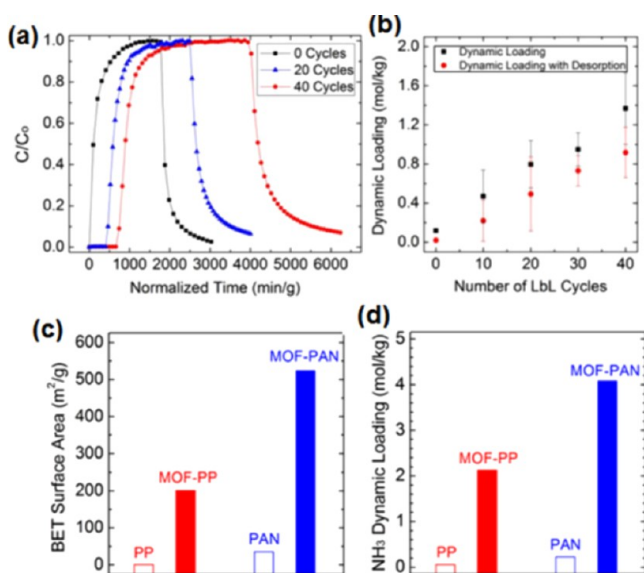


Figure 20. (a) NH_3 breakthrough curves and (b) NH_3 dynamic loading of ALD deposited PP microfiber after different HKUST-1 LbL growth cycles.⁴² Reprinted with permission from ref 42. Copyright 2015 The Royal Society of Chemistry. (c) BET area and (d) NH_3 dynamic loading of PP microfiber and PAN nanofiber with and without HKUST-1 coating. Adapted with permission from ref 43. Copyright 2015 American Chemical Society.

strategy using a dense ALD zinc oxide template. In this method, the dense zinc oxide layer first reacted with the copper salt to form a double hydroxyl salt, which then rapidly converted into HKUST-1. Compared with HKUST-1 coated PP microfibers from same approach, the HKUST-1/PAN nanofiber composite displayed a much higher NH_3 adsorption capacity, attributed to its higher MOF mass loading (Figure 20c,d). The high dynamic loadings of NH_3 as well as H_2S on these MOF-functionalized fiber mats suggest that these composites are highly promising for gas filters and protective suits.⁴³

The instability of HKUST-1 in the presence of water prevents the practical application of a HKUST-1 functionalized textile for toxic NH_3 gas capture under humid environments. To address this challenge, Parsons and team fabricated a water-stable copper porphyrin framework (Cu-TCPP) coating on a textile fiber, which could efficiently capture both NH_3 and 2-chloroethyl ethyl sulfide (CEES), a mustard gas simulant, under conditions with a relative humidity (RH) of 80%.⁵⁷

Moreover, the Cu-TCPP coating, sourced from a solid precursor, possessed a unique vertical morphology, which enhanced NH_3 adsorptive capacity by 3 times compared to the conventionally synthesized bulk MOF powder.

Another harmful gas pollutant includes SO_2 , which is a detrimental species to human health and can cause environmental problems like acid rain. Several studies demonstrated the efficacy of MOF/fiber composites for the removal of toxic SO_2 using MOF/fiber composites. Wang's group measured the uptake performance of their electrospun MOF/fiber composite using a dynamic adsorption test method.⁴¹ With a feed SO_2 concentration of 100 ppm and a flow rate of 50 mL min^{-1} , the HKUST-1/PAN nanofiber composites and UiO-66- NH_2 /PAN nanofiber composites exhibited a higher adsorption capacity of SO_2 compared to the pure PAN nanofiber. The authors credited the higher uptake in the MOF/fiber composite to the open copper sites or amino groups on ligands. In addition, the pressure drop in the MOF/fiber composite was relatively small, below 20 Pa at a flow rate of 50 mL min^{-1} in the test (Figure 21a). Remarkably, UiO-66- NH_2 /PAN maintained its capture capacity toward SO_2 after several adsorption cycles, possibly due to its chemical robustness (Figure 21a).⁴¹

Beyond the mere chemical adsorption of toxic gases, MOF-based composites can catalyze the degradation of harmful gases into benign species. Ozone (O_3) gas exists as an indoor air pollutant, especially in confined working places like printing rooms and offices. Wang and co-workers reported that MIL-100(Fe), possessing a high BET area and abundant Fe cluster active sites, showed high catalytic activity for the continuous decomposition of ozone.⁶⁶ They prepared a fibrous composite by hot-pressing the presynthesized MIL-100(Fe) nanoparticle onto a nonwoven fabric to yield a catalytically active composite (Figure 21b). The MOF/fiber composite degraded 200 ppb of ozone under a flow rate of 1000 mL min^{-1} and 45% relative humidity. Such composites with excellent catalytic performance under humidity have great potential in the production of personal protective devices, such as mask filters, against ozone pollution.

3.3. Toxic Gas Sensing. Beyond serving as efficient adsorbents, MOF/fiber composites can also act as indicators for the presence of hazardous gases. As referenced in the previous section regarding synthetic methods, Zhuang et al. printed a HKUST-1 pattern on a cotton textile fiber and reported the color change observed upon toxic gas exposure. After exposure to NH_3 , HCl, and H_2S , the turquoise blue color of the HKUST-1 pattern turned dark blue, yellow, and brown,

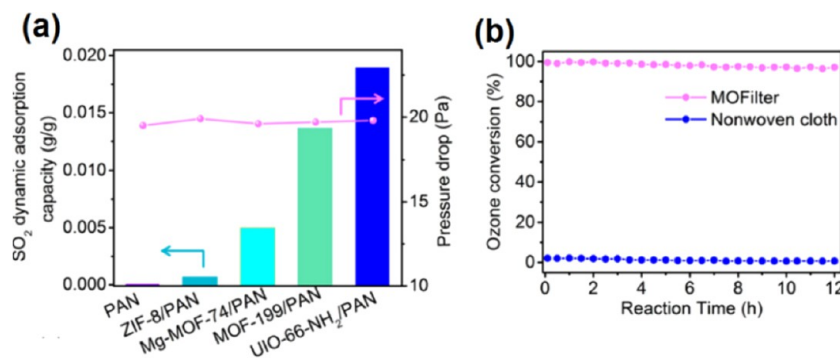


Figure 21. (a) SO_2 dynamic adsorption capacity and pressure drop of PAN nanofiber and MOF/PAN composites. (b) Catalytic decomposition of ozone (200 ppb) using a MIL-100(Fe)/fiber composite. Panel a: Adapted with permission from ref 41. Copyright 2016 American Chemical Society. Panel b: Adapted with permission from ref 66. Copyright 2018 John Wiley and Sons.

respectively, to serve as a visual indicator of the harmful gases present. However, the copper-based HKUST-1 lacked stability after exposure to these gases, preventing any reusability (Figure 22a).²⁹ Another study explored the more robust aluminum

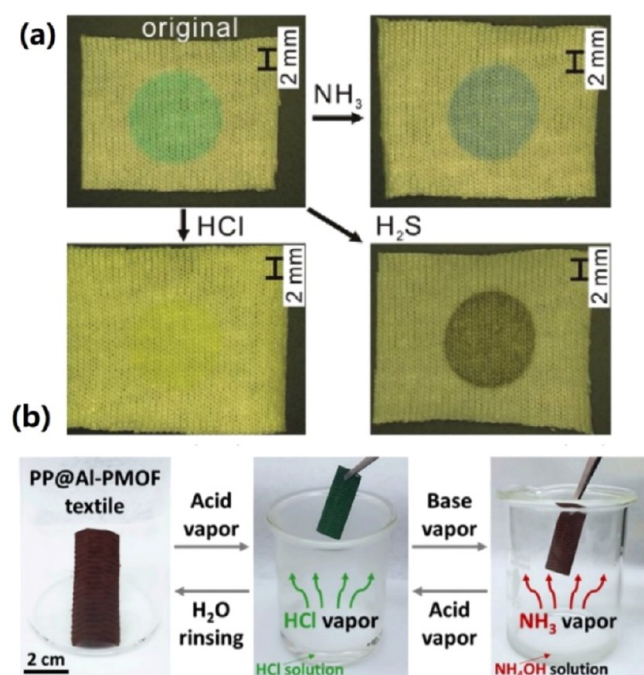


Figure 22. MOF/fiber used as a harmful gas sensor: (a) HKUST-1 pattern on cotton textile showing changes upon different toxic gas exposures. (b) A porphyrin-based MOF/fiber sensor showing reversible maroon–green color change to indicate the acid and base gases. Panel a: Adapted with permission from ref 29. Copyright 2013 John Wiley and Sons. Panel b: Adapted with permission from ref 58. Copyright 2020 Elsevier.

porphyrin framework/fiber (Al-PMOF/fiber) composite as a colorimetric textile base–acid sensor. The maroon color of the fibrous composite turned to a green hue when exposed to HCl vapor. Upon exposure to NH₃ vapor released from a NH₄OH solution, the composite reversibly and instantaneously returned to its original maroon color (Figure 22b).⁵⁸ The authors attributed the dramatic color change to the reversible protonation/deprotonation of the Lewis basic nitrogen sites on the porphyrin linker in Al-PMOF. A stirring test at 500 rpm for 10 min probed the strong adhesion of the MOF coating on the fiber surface and implied reusability in repeated sensing applications. The flexible and processable MOF/fiber sensors could supply protection to first responders for handling a toxic chemical spill.

Mirica and colleagues developed a facile approach for coating conductive two-dimensional (2D) metal–organic frameworks (MOFs) onto cotton fabrics through a direct solution-phase self-assembly in an aqueous reaction medium (Figure 23a).⁷⁴ These flexible and conductive MOF/cotton composites were employed to detect and differentiate toxic gaseous analytes (NO, H₂S, and H₂O) at parts per million levels. Importantly, the composite materials maintained their detection sensitivity when exposed to humidity (18% RH). With theoretical sub-parts-per-million detecting limits (0.16 ppm for NO and 0.23 ppm for H₂S), these fibrous composites were shown to be highly capable H₂S and NO detectors and chemiresistive sensors for these toxic gases (Figure 23b). Interestingly, the fibrous conductive MOF-

based composite showed good stability against washing. After washing the devices in deionized H₂O for 5 min and drying in air (12 h), their function was fully restored.

3.4. Catalytic Degradation of Chemical Warfare Agents. An emerging application of MOF powders, especially zirconium-based MOFs, includes the heterogeneous detoxification of ultratoxic chemical warfare agents (CWAs). Though several zirconium-based MOFs exhibited excellent catalytic activity in the hydrolysis of warfare agents or their related simulant, the poor processability of powdered MOFs hinders the real application of a such technology.^{16,17,70–73} Introducing catalytic Zr-MOFs onto flexible fiber substrates can produce protective clothes to safeguard soldiers, first-responders, and civilians from CWA threats.^{36,37,46,47,50}

López-Maya et al. investigated the catalytic degradation of nerve agent simulants using UiO-66/silk composite catalysts. The researchers first introduced MOF nanoparticles onto the silk nanofiber by spraying a MOF suspension followed by LiOtBu insertion.⁴⁶ The basic lithium alkoxide doped zirconium MOF composite catalyzed the hydrolysis of diisopropyl fluorophosphate (DIFP) and dimethyl methylphosphonate (DMMP), simulants for an organophosphorus nerve agent, and 2-chloroethyl ethyl sulfide (CEES), a mustard gas agent. The MOFs achieved half-lives of 20, 50, and 8 min for DIFP, DMNP, and CEES, respectively. A filter test verified the heterogeneous nature of these composite catalysts.

Parsons and co-workers further developed MOF/fiber composites for the degradation of CWAs. In their work, they synthesized conformal Zr-based MOF coatings, including UiO-66, UiO-66-NH₂, and UiO-67, on electrospun polyamide-6 (PA-6) nanofibers with ALD pretreatment to form a TiO₂ coating to promote nucleation.⁵¹ The researchers then utilized the prepared composites for the catalytic hydrolysis of a nerve agent simulant (DMNP) and the nerve agent soman, also known as GD. First, the hydrolysis reaction of DMNP in an aqueous buffer solution (pH = 10) was evaluated for both Zr-MOF coated nanofiber catalysts and free Zr-MOF nanoparticles. UiO-66-NH₂ and UiO-67 coatings on PA-6 nanofibers demonstrated ultrafast catalytic reaction rates for DMNP hydrolysis with half-lives less than 8 min. Importantly, the MOFs bonded onto fibrous substrates showed comparable catalytic activity with respect to free MOF nanoparticles, while the PA-6 nanofiber with only the TiO₂ ALD coating yielded a half-life of about 20 h, verifying the catalytic activity of the MOF layer. Then, the UiO-66, UiO-66-NH₂, and UiO-67 coated PA-6 fibers degraded GD with resulting half-lives of 3.0, 3.7, and 2.3 min, respectively. This work provided the first demonstration of the catalytic degradation of a real nerve agent (GD) using a MOF/fiber composite under ambient humidity.

Recently, our group reported the first example of coating the 6-connected MOF-808 onto a commercial polyester (PET) fiber as the functional layer for the catalytic hydrolysis of GD and the less toxic DMNP simulant.³⁸ By tuning the synthesis time, we prepared MOF-808/PET composites with MOF loadings of 6.5, 12, and 22%, denoted as MOF-808_{6.5%}/PET, MOF-808_{12%}/PET, and MOF-808_{22%}/PET. The MOF-808_{6.5%}/PET composite demonstrated a total conversion after 1.5 min; we extrapolated the initial half-lives of MOF-808_{6.5%}/PET, MOF-808_{12%}/PET, and MOF-808_{22%}/PET as <0.5, <1, and 3 min, respectively (Figure 24). UiO-66-NH₂/PET, with a MOF loading of 8%, reported a relatively longer half-life of 5 min. Our team attributed the improvement in catalytic activity of the MOF-808/fiber composite to the lower connectivity on the Zr

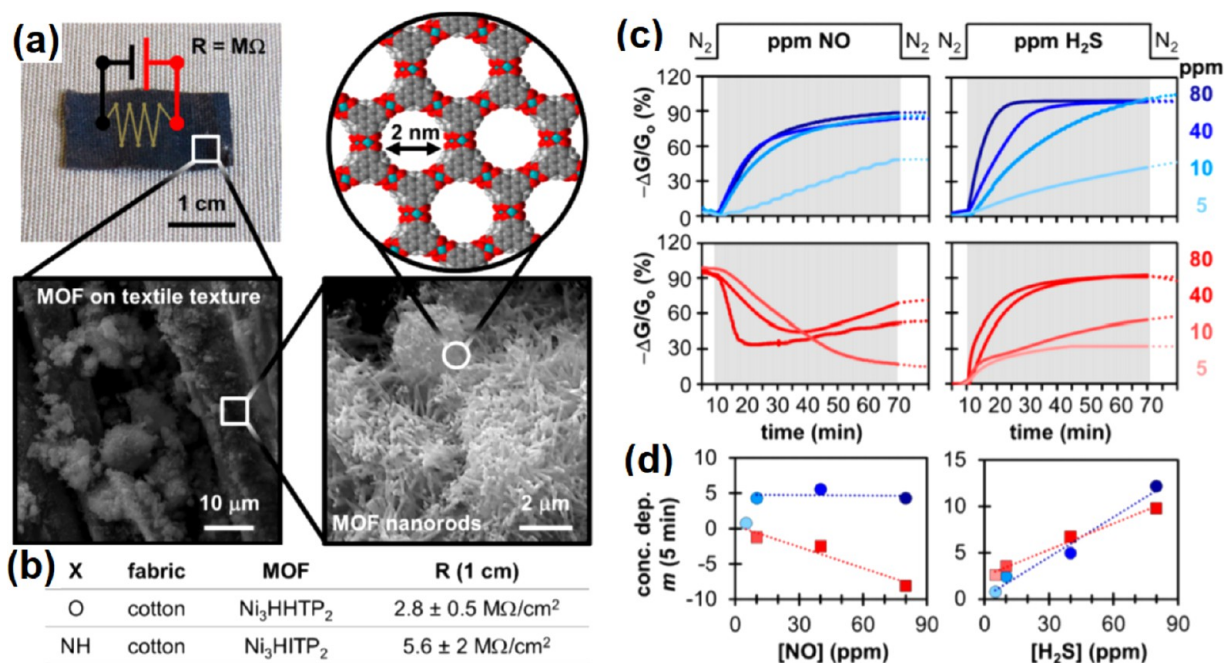


Figure 23. (a) Conductive triphenylene MOF-based fibrous composite. (b) Sheet resistance of the two conductive MOF/fiber composites. (c) Representative response for Ni₃HITP₂ (blue) and Ni₃HHTP₂ (red) based sensors, exposing to NO or H₂S. (d) Slope (m) of first 5 min of conductive MOF-based fibrous sensor response versus concentration of NO (left) and H₂S (right). Adapted with permission from ref 74. Copyright 2017 American Chemical Society.

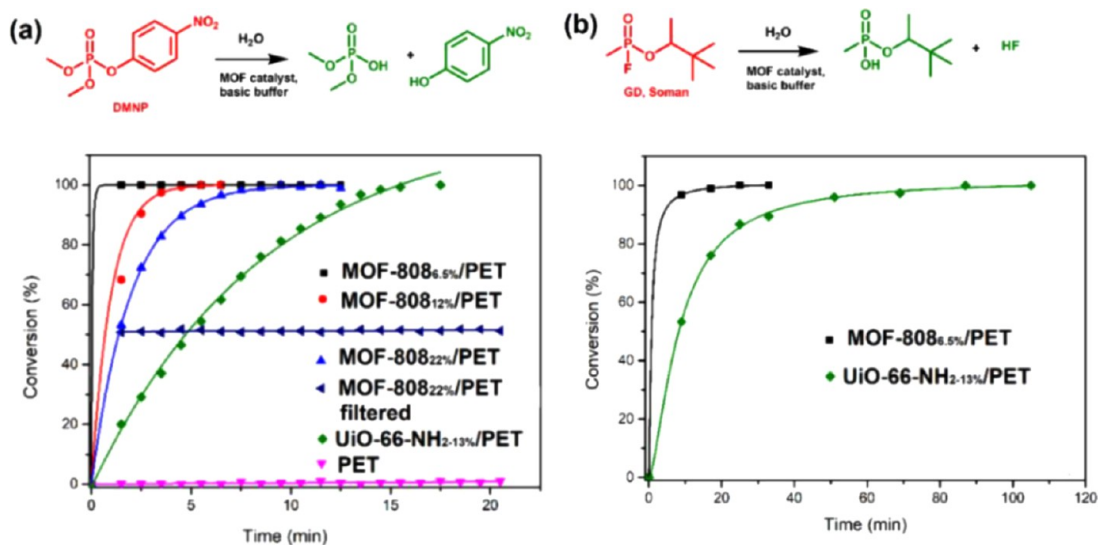


Figure 24. (a) DMNP and (b) GD catalytic hydrolysis reaction kinetics using Zr-MOF/fiber prepared from a template-free aqueous synthetic approach. Adapted with permission from ref 38. Copyright 2019 American Chemical Society.

cluster (6-connected) in MOF-808, which supply more Lewis acid catalytic sites for the hydrolysis reaction. Encouragingly, the MOF-808/fiber and UiO-66-NH₂/fiber composites could efficiently degrade GD with half-lives of 2 and 8 min, respectively (Figure 24b). The MOF-808/fiber composites exhibited the best catalytic performance for DMNP and GD hydrolysis as compared with that of the previously reported MOF/fiber composites. In addition, the catalytic performance remained unchanged after 6 months of storage in air or 24 h of stirring (400 rpm) in water, indicating the excellent stability and durability of the MOF/fiber composite catalyst. The retention of CWAs through protective clothing material is an essential step for the catalytic degradation and the protective efficiency.

Simply, a longer retention time of the toxic CWAs affords more time to accomplish the catalytic degradation of the agent. We demonstrated the favorable barrier performance of Zr-MOF/fiber composites according to ASTM F739-12 test protocols, where 300 mg m⁻³ CEES, as the analyte, was fed across the Zr-MOF/fiber composite (1 in. in diameter) at a flow rate of 300 mL min⁻¹. According to the above test standard, UiO-66-NH₂/PET (loading 27%) and MOF-808/PET (loading 22%) displayed effective protection performances of >50 and 126 min, respectively, and permeation rates of CEES under the limit of 0.1 μg min⁻¹ cm⁻².

These above-mentioned studies on the catalytic hydrolysis of organophosphorus nerve agents require the addition of water

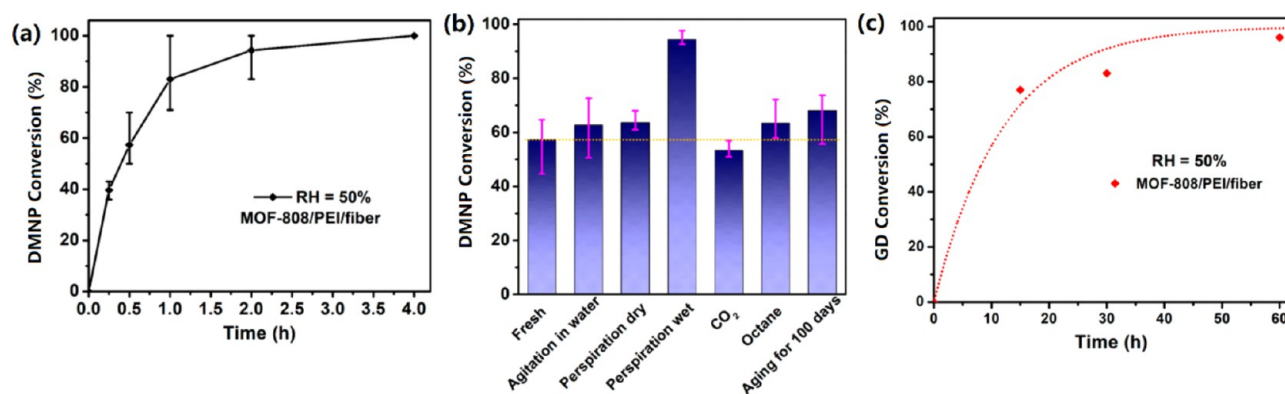


Figure 25. Solid state catalytic hydrolysis of DMNP using a MOF-808/PEI/fiber composite. (a) DMNP kinetic profile and (b) performance under different challenges, including under agitation in water, after perspiration exposure, in a simulated CO₂-rich and gasoline-rich atmosphere, and after storage in air for 100 days. (c) Kinetic profile of catalytic hydrolysis of soman (GD) using MOF-808/PEI/fiber composites. Adapted with permission from ref 67. Copyright 2019 American Chemical Society.

and volatile bases, which can only be accommodated for the decontamination of large stockpiles. By incorporating the nonvolatile polymeric base PEI into the composite and using the water molecules in the MOF pores adsorbed from the atmosphere, we circumvented these problems to create a MOF/PEI/fiber composite practical for field use.⁶⁷ Kinetic studies of DMNP hydrolysis using MOF-808/PEI/fiber composite as a catalyst under 50% relative humidity (RH) resulted in an initial half-life of about 0.4 h (Figure 25), similar to the activity of some Zr-MOF-based catalysts in volatile organic bases buffer solution. The solid-state catalytic hydrolysis of nerve agent soman (GD) exhibited an encouraging shorter half-life of only 12 min under RH = 50%. To probe whether real-world conditions would adversely impact the performance of these composites, we mimicked exposure to sweat, atmospheric CO₂, and diesel, which showed no decline in reactivity. Furthermore, we demonstrated the durability of the composites having a prolonged shelf life of over 100 days. With the formation of MOF/fiber composites using scalable and generalizable procedures, we successfully illustrated how these materials can move toward industrial applications. This is the first MOF-based protective fiber that efficiently degrades a nerve agent and a related simulant without added base or liquid water.

Additionally, our team reported the efficiency of chromophore linkers such as porphyrin and pyrene units present within PCN-222 and NU-1000, respectively, generate singlet oxygen for the selective oxidation of mustard gas into nontoxic sulfoxide.^{16,17} Parsons and researchers extended the selective oxidation of a mustard gas simulant using an alumina porphyrin framework (Al-PMOF) coated on PP fiber (denoted as PP@Al-PMOF), derived from an ALD alumina precursor layer.⁵⁸ Upon LED irradiation, PP@Al-PMOF accomplished fast and selective oxidation to form the sulfoxide species with a half-life of 4 min while the Al-PMOF particle and TCPP linker alone yielded respective half-lives of 16 and 6 min (Figure 26). The authors credited the superior performance of PP@Al-PMOF to an intriguing, radial growth and subsequent orientation of the MOF on the fiber that limited light scattering. While the toxic and volatile media for singlet oxygen generation is not safe or practical for users, this work serves as a step toward creating MOF-functionalized protective clothing against mustard gas. Practical gear requires further work to synthesize catalytic composites active under ambient conditions.

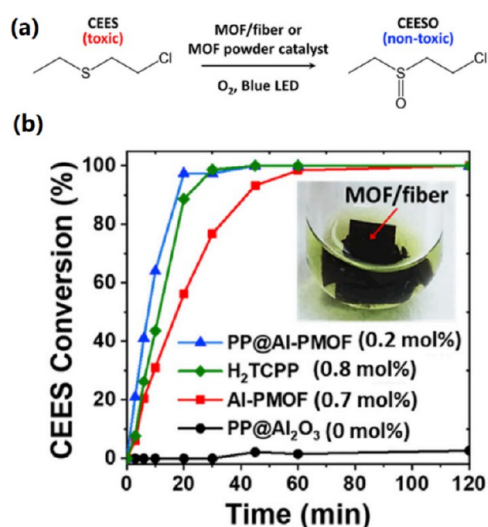


Figure 26. Selective photocatalytic oxidation of mustard gas simulant, CEES, under blue LED light using aluminum porphyrin framework catalysts and its fibrous composite. Adapted with permission from ref 58. Copyright 2020 Elsevier.

3.5. Healthcare Application. The health-care field offers targeted applications for MOF-based composites such as controlled drug release and antibacterial materials. For example, the controlled release of nitric oxide (NO) is critical in the biomedical field because of its bioactivity in antiplatelet aggregation as well as its antibacterial and anti-inflammatory effects. However, challenges remain in engineering a controlled release.^{75–77} Reynolds et al. discovered that the copper-based MOF, HKUST-1, showed effective catalytic activity for the generation of NO from a S-nitrosocysteine precursor.⁷⁸ With this strategy in mind, they successfully developed a HKUST-1/cotton composite for NO release (Figure 27).⁴⁸ The HKUST-1 coated cotton fiber triggered the effective generation of NO (7.1 ± 1.2 μmol NO/mg MOF) over a long release period. The HKUST-1 coating on the cotton fiber exhibited a shorter induction period compared to a mixed matrix membrane (MMM) containing the same amount of HKUST-1. Likely, the greater accessibility of the catalyst sites on the cotton fiber likely correlated with the faster diffusion of the substrates. Diffuse reflectance UV–vis spectroscopy and ICP-AES measurements demonstrated coating stability after the catalytic reaction. The

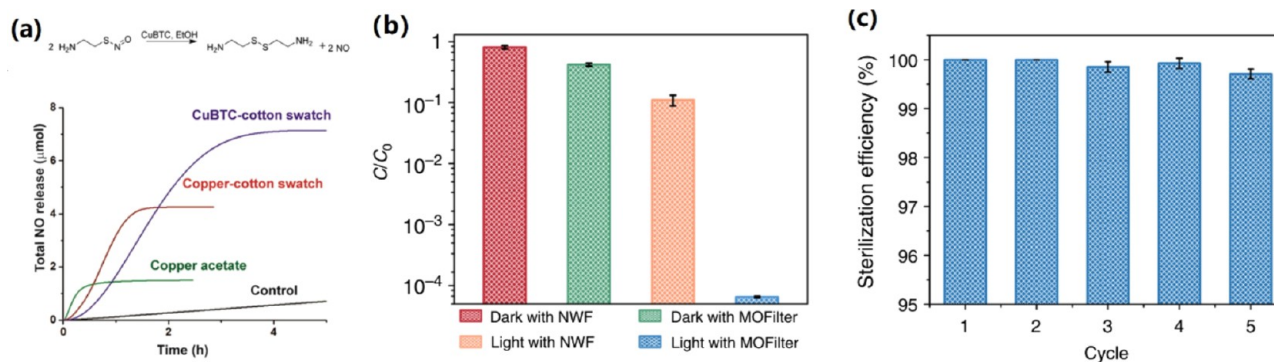


Figure 27. MOF/fiber composites' application in healthcare fields. (a) Catalytic release of NO from a S-nitrosocysteamine precursor using different catalysts. (b) Antibacterial performance and (c) the reusability of ZIF-8/fiber filter under simulated sunlight. Panel a: Adapted with permission from ref 48. Copyright 2015 American Chemical Society. Panels b and c: Adapted with permission from ref 63. Copyright 2019 Nature Publishing Group.

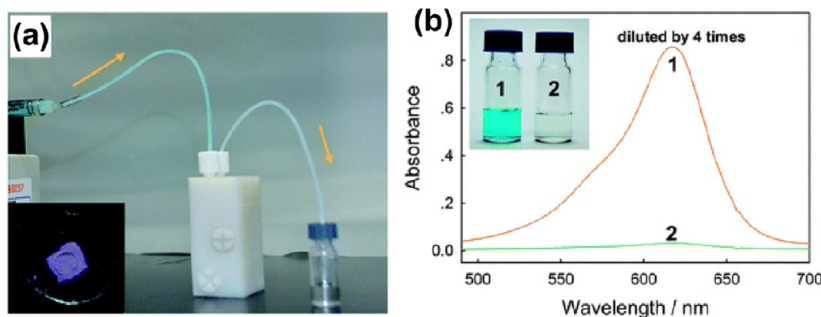


Figure 28. (a) Photograph image of a filtration device using ZIF-67/fiber composite (insert) as the filler. (b) The UV-visible spectra and the photograph image of malachite green solution (1) before and (2) after filtration. Adapted with permission from ref 40. Copyright 2018 The Royal Society of Chemistry.

excellent performance of the HKUST-1/cotton composite introduces a promising catalyst for the controlled release of NO.

Densely populated environments, including hospitals and nursing centers, coupled with warm and humid temperatures lead to favorable conditions for pathogenic microorganisms—including bacteria, viruses, and fungi—to grow, which yields serious complications. With the contemporary outbreak of SARS-CoV-2 (COVID-19), it is evident that pathogens pose serious threats to global society. Previously, MOFs served as disinfectants against pathogens.⁶³ The successful immobilization of MOFs onto fibers renders these composites as viable routes for the production of bioprotective clothing and masks. Toward this end, Wang's group developed a ZIF-8/fiber composite, named MOFilter, for application as a light induced antibacterial material. The MOF/fiber composite filters exhibited remarkable antibacterial performances, with disinfection efficiencies >99.99% against airborne bacteria in 30 min under simulated sunlight irradiation (Figure 27b). A mechanistic study revealed that photoelectrons trapped at the zinc cluster within the ZIF-8 framework via ligand to metal charge transfer (LMCT) could reduce oxygen to generate reactive oxygen species (ROS), which are strongly biocidal to bacteria. The disinfection efficiency remained intact after five cycles, indicating ample reusability (Figure 27c). However, the necessity of sunlight may hinder the practical application of these composites for use under dark environments or at night.

3.6. Water Purification. Given their sufficient processability and permanent porosity, MOF/fiber composites have potential for the removal of pollutants from water. Moreover, the fibrous composites allow for a more facile recovery, as compared to a powdered MOF absorbent, for water purification

applications. Fu et al. explored the MOF-nanofiber composites' efficacy in the removal of toxic heavy metal ions and organic dyes (Figure 28).⁴⁰ In that study, electrospun silk nanofibers served as the substrate for MOF growth. The MOF coating on fiber achieved the same uptake capability of that of free MOF powders, indicating the high accessibility of the active site in the MOF coating. For example, the ZIF-67 coating on the component displayed a normalized malachite green adsorption of 2124 mg g⁻¹, comparable to the uptake capacity of the free MOF powder. The MOF/fiber composites removed the two kinds of heavy metal ions studied, As(V) and Cr(VI), as well as organic dyes, rhodamine B and malachite green, with nearly 100% efficiency. The researchers assembled a filtration device using the composite as the functional filter for the continuous adsorption of malachite green. The device obtained a removal efficiency of about 100% after one cycle. The blue color of simulated polluted water turned almost colorless after filtration with the ZIF-67/silk nanofiber composite (Figure 28b).

Additionally, Wang and team built another filtration device through employing the MOF-carbon fiber composites, prepared using the hot-pressing method, as the filter filler for continuous adsorption of highly toxic As^V ion from water.⁴⁵ ZIF-8/carbon fiber, ZIF-9/carbon fiber, and ZIF-67/carbon fiber composites demonstrated impressive uptake capacities of 27.2, 53.1, and 32.6 mg g⁻¹ m⁻², respectively, while uncoated carbon fiber cloth only showed a nominal capacity of 4.3 mg m⁻².

4. CONCLUSIONS AND OUTLOOK

The fabrication of MOF/fiber composites is critical for practical industrial applications, such as functional filters, heterogeneous catalysts, sensors, and protective gear. Although different

research teams have achieved the small-scale development of functional MOF/fiber composites, the industrial production and application of MOF/fiber composites under relevant conditions remain in a primitive stage. Consequently, emerging strategies for the facile and large-scale fabrication of MOF/fiber composites are critical for the implementation of such technologies in industrial processing. Moreover, the design of multicomponent MOF/fiber composites can accomplish more complex, multitask systems. On the basis of the advances in the fabrication of MOF/fiber composites for pollutant removal and protection against chemical warfare agents, we identify and present below our outlook on the future directions for this important and powerful field of research.

(1) The expansion of MOF/fiber composite fabrication methods to different metal-containing MOFs, such as water stable iron-based, aluminum-based, and zirconium-based MOFs, will extend the possible applications for such hybrid systems.

(2) Currently, most synthetic procedures for MOF/fiber composites require near reflux temperatures, which limits the use of thermally sensitive fibers, such as cotton. Therefore, the design of milder synthesis methods, such as at room temperature in aqueous media, will more readily allow for MOF coatings on widely used and thermally sensitive fibers.

(3) The prepared MOF/fiber composites served as excellent barrier function materials against CWA simulant analytes. Further investigation, however, should examine the diffusion of real warfare agents, such as mustard gas and GD, through the family of porous composites to elucidate differences arising from CWA molecular size and hydrophobicity. Furthermore, investigating the destruction of mixed warfare agents using MOF/fiber composites will provide a more accurate description of the protection efficiency of these composites under relevant conditions.

(4) Relevant practical conditions should be considered when designing a MOF/fiber composite. For example, certain functional MOF/fiber composite materials will only work under specific conditions, such as sunlight for the photoinduced antibacterial MOF/fiber filter. Thus, a more universal functional MOF/fiber material will be more likely to serve as a feasible technology.

(5) Binary MOF/fiber composites only contain a pure MOF layer and a fiber substrate, which may limit their applications. Polybasic composites, which introduce polymers, metal nanoparticles, and biomacromolecules into MOF/fiber composite systems, may enable a more synergistic and enhanced functional material. However, polybasic MOF-based composites still remain underexplored with few reported examples at the time of this review.

(6) The degradation of MOF coatings on fiber substrates during use could hinder the functionality of the composites, while the free metal ions and organic ligands could leach from the composite to impart negative effects to the user and/or environment. Likewise, commonly used hazardous solvents, such as DMSO and DMF, are easily trapped in the MOFs pores during MOF/fiber composite synthesis. Their retention in the composite becomes a potential risk for the inhalation of these vapors, especially within health-care materials and protection gear. Therefore, further studies investigating and mitigating residual solvent could alleviate any related health risks.

(7) Further study of critical properties such as mass loading, BET area, coverage, and uniformity, will better evaluate the properties of MOF/fiber composites. In particular, the

normalized BET area of the MOF coating component should serve as an important quality control criterion.

(8) The structure–property relationships for MOF/fiber composites, beyond the identity of the MOF or fiber, are also crucial and should be evaluated as different applications might require composites with varying properties. For example, increasing MOF loading has been considered as a strategy for increasing the toxic gas removal capacity of the composites; however, this might not have a significant effect for sensing applications. Additionally, studies on the synergetic effect of composites that utilize the fiber material beyond a support to introduce flexibility will advance the future of functional MOF/fiber composite materials.

■ AUTHOR INFORMATION

Corresponding Authors

John H. Xin – *Research Centre for Smart Wearable Technology, Institute of Textiles and Clothing, The Hong Kong Polytechnic University, Hong Kong, SAR 999077, China; Email: tcxinjh@polyu.edu.hk*

Omar K. Farha – *Department of Chemistry and International Institute for Nanotechnology, Northwestern University, Evanston, Illinois 60208, United States; orcid.org/0000-0002-9904-9845; Email: o-farha@northwestern.edu*

Authors

Kaikai Ma – *Department of Chemistry and International Institute for Nanotechnology, Northwestern University, Evanston, Illinois 60208, United States; Research Centre for Smart Wearable Technology, Institute of Textiles and Clothing, The Hong Kong Polytechnic University, Hong Kong, SAR 999077, China; orcid.org/0000-0003-0414-4397*

Karam B. Idrees – *Department of Chemistry and International Institute for Nanotechnology, Northwestern University, Evanston, Illinois 60208, United States; orcid.org/0000-0002-9603-3952*

Florencia A. Son – *Department of Chemistry and International Institute for Nanotechnology, Northwestern University, Evanston, Illinois 60208, United States; orcid.org/0000-0002-7524-3774*

Rodrigo Maldonado – *Department of Chemistry and International Institute for Nanotechnology, Northwestern University, Evanston, Illinois 60208, United States*

Megan C. Wasson – *Department of Chemistry and International Institute for Nanotechnology, Northwestern University, Evanston, Illinois 60208, United States; orcid.org/0000-0002-9384-2033*

Xuan Zhang – *Department of Chemistry and International Institute for Nanotechnology, Northwestern University, Evanston, Illinois 60208, United States; orcid.org/0000-0001-8214-7265*

Xingjie Wang – *Department of Chemistry and International Institute for Nanotechnology, Northwestern University, Evanston, Illinois 60208, United States; orcid.org/0000-0002-5802-9944*

Elissa Shehayeb – *Department of Chemistry, American University of Beirut, Beirut 1107-2020, Lebanon*

Areej Merhi – *Department of Chemistry, American University of Beirut, Beirut 1107-2020, Lebanon*

Bilal R. Kaafarani – *Department of Chemistry, American University of Beirut, Beirut 1107-2020, Lebanon*

Timur Islamoglu – *Department of Chemistry and International Institute for Nanotechnology, Northwestern University, Evanston,*

Illinois 60208, United States; orcid.org/0000-0003-3688-9158

Complete contact information is available at:
<https://pubs.acs.org/10.1021/acs.chemmater.0c02379>

Notes

The authors declare no competing financial interest.

ACKNOWLEDGMENTS

The authors acknowledge the financial support from the Defense Threat Reduction Agency (HDTRA1-18-1-0003 and HDTRA1-19-1-0007), the Army Research Office (W911NF1910340), the Inorganometallic Catalyst Design Center, an Energy Frontier Research Center funded by the DOE, Office of Science, Basic Energy Sciences (DE-SC0012702), and the Northwestern University Institute for Catalysis in Energy Processes (ICEP), funded by the DOE, Office of Basic Energy Sciences (Award Number DE-FG02-03ER15457). M.C.W. is supported by the NSF Graduate Research Fellowship under grant DGE-1842165. F.A.S. is supported by the Department of Defense (DoD) through the National Defense Science & Engineering Graduate (NDSEG) Fellowship Program. J.H.X. acknowledges the support from the General Research Fund of the Research Grants Council of the Hong Kong SAR Government (GRF 15208420).

REFERENCES

- (1) Furukawa, H.; Cordova, K. E.; O’Keeffe, M.; Yaghi, O. M. The Chemistry and Applications of Metal–Organic Frameworks. *Science* **2013**, *341* (6149), 1230444.
- (2) Li, H.; Eddaoudi, M.; O’Keeffe, M.; Yaghi, O. M. Design and Synthesis of an Exceptionally Stable and Highly Porous Metal–Organic Framework. *Nature* **1999**, *402*, 276–279.
- (3) Zhou, H.-C.; Kitagawa, S. Metal–Organic Frameworks (MOFs). *Chem. Soc. Rev.* **2014**, *43* (16), 5415–5418.
- (4) Park, K. S.; Ni, Z.; Côté, A. P.; Choi, J. Y.; Huang, R.; Uribe-Romo, F. J.; Chae, H. K.; O’Keeffe, M.; Yaghi, O. M. Exceptional Chemical and Thermal Stability of Zeolitic Imidazolate Frameworks. *Proc. Natl. Acad. Sci. U. S. A.* **2006**, *103* (27), 10186–10191.
- (5) James, S. L. Metal–Organic Frameworks. *Chem. Soc. Rev.* **2003**, *32* (5), 276–288.
- (6) Farha, O. K.; Eryazici, I.; Jeong, N. C.; Hauser, B. G.; Wilmer, C. E.; Sarjeant, A. A.; Snurr, R. Q.; Nguyen, S. T.; Yazaydin, A. Ö.; Hupp, J. T. Metal–Organic Framework Materials with Ultrahigh Surface Areas: Is the Sky the Limit? *J. Am. Chem. Soc.* **2012**, *134* (36), 15016–15021.
- (7) Chen, Z.; Li, P.; Anderson, R.; Wang, X.; Zhang, X.; Robison, L.; Redfern, L. R.; Moribe, S.; Islamoglu, T.; Gomez-Gualdrón, D. A.; Yildirim, T.; Stoddart, J. F.; Farha, O. K. Balancing Volumetric and Gravimetric Uptake in Highly Porous Materials for Clean Energy. *Science* **2020**, *368* (6488), 297–303.
- (8) Li, J.-R.; Kuppler, R. J.; Zhou, H.-C. Selective Gas Adsorption and Separation in Metal–Organic Frameworks. *Chem. Soc. Rev.* **2009**, *38* (5), 1477–1504.
- (9) Rosi, N. L.; Eckert, J.; Eddaoudi, M.; Vodak, D. T.; Kim, J.; O’Keeffe, M.; Yaghi, O. M. Hydrogen Storage in Microporous Metal–Organic Frameworks. *Science* **2003**, *300* (5622), 1127–1129.
- (10) Sumida, K.; Rogow, D. L.; Mason, J. A.; McDonald, T. M.; Bloch, E. D.; Herm, Z. R.; Bae, T.-H.; Long, J. R. Carbon Dioxide Capture in Metal–Organic Frameworks. *Chem. Rev.* **2012**, *112* (2), 724–781.
- (11) Lin, R.-B.; Xiang, S.; King, H.; Zhou, W.; Chen, B. Exploration of Porous Metal–Organic Frameworks for Gas Separation and Purification. *Coord. Chem. Rev.* **2019**, *378*, 87–103.
- (12) Murray, L. J.; Dinca, M.; Long, J. R. Hydrogen Storage in Metal–Organic Frameworks. *Chem. Soc. Rev.* **2009**, *38* (5), 1294–1314.
- (13) Kirlikovali, K. O.; Chen, Z.; Islamoglu, T.; Hupp, J. T.; Farha, O. K. Zirconium-Based Metal–Organic Frameworks for the CatalyticHydrolysis of Organophosphorus Nerve Agents. *ACS Appl. Mater. Interfaces* **2020**, *12* (13), 14702–14720.
- (14) Xiao, J.-D.; Jiang, H.-L. Metal–Organic Frameworks for Photocatalysis and Photothermal Catalysis. *Acc. Chem. Res.* **2019**, *52* (2), 356–366.
- (15) Wasson, M. C.; Buru, C. T.; Chen, Z.; Islamoglu, T.; Farha, O. K. Metal–Organic Frameworks: A Tunable Platform to Access Single-Site Heterogeneous Catalysts. *Appl. Catal., A* **2019**, *586*, 117214.
- (16) Liu, Y.; Buru, C. T.; Howarth, A. J.; Mahle, J. J.; Buchanan, J. H.; DeCoste, J. B.; Hupp, J. T.; Farha, O. K. Efficient and Selective Oxidation of Sulfur Mustard Using Singlet Oxygen Generated by a Pyrene-Based Metal–Organic Framework. *J. Mater. Chem. A* **2016**, *4* (36), 13809–13813.
- (17) Liu, Y.; Howarth, A. J.; Hupp, J. T.; Farha, O. K. Selective Photooxidation of a Mustard–Gas Simulant Catalyzed by a Porphyrinic Metal–Organic Framework. *Angew. Chem., Int. Ed.* **2015**, *54* (31), 9001–9005.
- (18) DeCoste, J. B.; Peterson, G. W. Metal–Organic Frameworks for Air Purification of Toxic Chemicals. *Chem. Rev.* **2014**, *114* (11), 5695–5727.
- (19) Barea, E.; Montoro, C.; Navarro, J. A. Toxic Gas Removal–Metal–Organic Frameworks for the Capture and Degradation of Toxic Gases and Vapours. *Chem. Soc. Rev.* **2014**, *43* (16), 5419–5430.
- (20) Li, J.; Wang, X.; Zhao, G.; Chen, C.; Chai, Z.; Alsaedi, A.; Hayat, T.; Wang, X. Metal–Organic Framework-Based Materials: Superior Adsorbents for the Capture of Toxic and Radioactive Metal Ions. *Chem. Soc. Rev.* **2018**, *47*, 2322–2356.
- (21) Islamoglu, T.; Chen, Z.; Wasson, M. C.; Buru, C. T.; Kirlikovali, K. O.; Afrin, U.; Mian, M. R.; Farha, O. K. Metal–Organic Frameworks against Toxic Chemicals. *Chem. Rev.* **2020**, DOI: 10.1021/acs.chemrev.9b00828.
- (22) Liu, X.; Fu, W.; Bouwman, E. One-Step Growth of Lanthanoid Metal–Organic Framework (MOF) Films under Solvothermal Conditions for Temperature Sensing. *Chem. Commun.* **2016**, *52*, 6926–6929.
- (23) Kreno, L. E.; Leong, K.; Farha, O. K.; Allendorf, M.; Van Duyne, R. P.; Hupp, J. T. Metal–Organic Framework Materials as Chemical Sensors. *Chem. Rev.* **2012**, *112* (2), 1105–1125.
- (24) Liu, J.; Woll, C. Surface-Supported Metal–Organic Framework Thin Films: Fabrication Methods, Applications, and Challenges. *Chem. Soc. Rev.* **2017**, *46* (19), 5730–5770.
- (25) Kitao, T.; Zhang, Y.; Kitagawa, S.; Wang, B.; Uemura, T. Hybridization of MOFs and Polymers. *Chem. Soc. Rev.* **2017**, *46* (11), 3108–3133.
- (26) Bradshaw, D.; Garai, A.; Huo, J. Metal–Organic Framework Growth at Functional Interfaces: Thin Films and Composites for Diverse Applications. *Chem. Soc. Rev.* **2012**, *41* (6), 2344–2381.
- (27) Zhang, Y.; Feng, X.; Li, H.; Chen, Y.; Zhao, J.; Wang, S.; Wang, L.; Wang, B. Photoinduced Postsynthetic Polymerization of a Metal–Organic Framework toward a Flexible Stand-Alone Membrane. *Angew. Chem., Int. Ed.* **2015**, *54* (14), 4259–4263.
- (28) Mao, Y. Y.; Li, G. R.; Guo, Y.; Li, Z. P.; Liang, C. D.; Peng, X. S.; Lin, Z. Foldable Interpenetrated Metal–Organic Frameworks/Carbon Nanotubes Thin Film for Lithium–Sulfur Batteries. *Nat. Commun.* **2017**, *8*, 14628.
- (29) Zhuang, J.-L.; Ar, D.; Yu, X.-J.; Liu, J.-X.; Terfort, A. Patterned Deposition of Metal–Organic Frameworks onto Plastic, Paper, and Textile Substrates by Inkjet Printing of a Precursor Solution. *Adv. Mater.* **2013**, *25* (33), 4631–4635.
- (30) Pinto, M. L.; Dias, S.; Pires, J. Composite MOF Foams: The Example of UiO-66/Polyurethane. *ACS Appl. Mater. Interfaces* **2013**, *5* (7), 2360–2363.
- (31) Aguado, S.; Canivet, J.; Farrusseng, D. Facile Shaping of an Imidazolate-Based MOF on Ceramic Beads for Adsorption and Catalytic Applications. *Chem. Commun.* **2010**, *46* (42), 7999–8001.
- (32) Reboul, J.; Furukawa, S.; Horike, N.; Tsotsalas, M.; Hirai, K.; Uehara, H.; Kondo, M.; Louvain, N.; Sakata, O.; Kitagawa, S. Mesoscopic Architectures of Porous Coordination Polymers Fabricated by Pseudomorphic Replication. *Nat. Mater.* **2012**, *11*, 717–723.

- (33) Biemmi, E.; Scherb, C.; Bein, T. Oriented Growth of the Metal Organic Framework $\text{Cu}_3(\text{BTC})_2(\text{H}_2\text{O})_3 \cdot x\text{H}_2\text{O}$ Tunable with Functionalized Self-Assembled Monolayers. *J. Am. Chem. Soc.* **2007**, *129* (26), 8054–8055.
- (34) McCarthy, D. L.; Liu, J.; Dwyer, D. B.; Troiano, J. L.; Boyer, S. M.; DeCoste, J. B.; Bernier, W. E.; Jones, W. E., Jr. Electrospun Metal-Organic Framework Polymer Composites for the Catalytic Degradation of Methyl Paraxon. *New J. Chem.* **2017**, *41*, 8748–8753.
- (35) Abbasi, A. R.; Akhbari, K.; Morsali, A. Dense Coating of Surface Mounted Cubic Metal-Organic Framework Nanostructures on Silk Fibers, Prepared by Layer-By-Layer Method under Ultrasound Irradiation with Antibacterial Activity. *Ultrason. Sonochem.* **2012**, *19* (4), 846–852.
- (36) Boehringer, B.; Fischer, R.; Lohe, M. R.; Rose, M.; Kaskel, S.; Küsgens, P. *MOF Shaping and Immobilization*; Farrusseng, D., Ed.; Wiley-VCH Verlag GmbH: Weinheim, 2011.
- (37) Liu, C.; Wu, Y. N.; Morlay, C.; Gu, Y. F.; Gebremariam, B.; Yuan, X.; Li, F. T. General Deposition of Metal-Organic Frameworks on Highly Adaptive Organic-Inorganic Hybrid Electrospun Fibrous Substrates. *ACS Appl. Mater. Interfaces* **2016**, *8* (4), 2552–2561.
- (38) Ma, K.; Islamoglu, T.; Chen, Z.; Li, P.; Wasson, M. C.; Chen, Y.; Wang, Y.; Peterson, G. W.; Xin, J. H.; Farha, O. K. Scalable and Template-Free Aqueous Synthesis of Zirconium-Based Metal-Organic Framework Coating on Textile Fiber. *J. Am. Chem. Soc.* **2019**, *141* (39), 15626–15633.
- (39) Zhao, J.; Losego, M. D.; Lemaire, P. C.; Williams, P. S.; Gong, B.; Atanasov, S. E.; Blevins, T. M.; Oldham, C. J.; Walls, H. J.; Shepherd, S. D.; Browe, M. A.; Peterson, G. W.; Parsons, G. N. Highly Adsorptive, MOF-Functionalized Nonwoven Fiber Mats for Hazardous Gas Capture Enabled by Atomic Layer Deposition. *Adv. Mater. Interfaces* **2014**, *1* (4), 1400040.
- (40) Li, Z.; Zhou, G.; Dai, H.; Yang, M.; Fu, Y.; Ying, Y.; Li, Y. Biomimetic Preparation of Hybrid Membranes with Ultra-High Loading of Pristine Metal-Organic Frameworks Grown on Silk Nanofibers for Hazard Collection in Water. *J. Mater. Chem. A* **2018**, *6* (8), 3402–3413.
- (41) Zhang, Y.; Yuan, S.; Feng, X.; Li, H.; Zhou, J.; Wang, B. Preparation of Nanofibrous Metal–Organic Framework Filters for Efficient Air Pollution Control. *J. Am. Chem. Soc.* **2016**, *138* (18), 5785–5788.
- (42) Zhao, J.; Gong, B.; Nunn, W. T.; Lemaire, P. C.; Stevens, E. C.; Sidi, F. I.; Williams, P. S.; Oldham, C. J.; Walls, H. J.; Shepherd, S. D.; Browe, M. A.; Peterson, G. W.; Losego, M. D.; Parsons, G. N. Conformal and Highly Adsorptive Metal–Organic Framework Thin Films via Layer-By-Layer Growth on ALD-Coated Fiber Mats. *J. Mater. Chem. A* **2015**, *3* (4), 1458–1464.
- (43) Zhao, J.; Nunn, W. T.; Lemaire, P. C.; Lin, Y.; Dickey, M. D.; Oldham, C. J.; Walls, H. J.; Peterson, G. W.; Losego, M. D.; Parsons, G. N. Facile Conversion of Hydroxy Double Salts to Metal-Organic Frameworks Using Metal Oxide Particles and Atomic Layer Deposition Thin-Film Templates. *J. Am. Chem. Soc.* **2015**, *137* (43), 13756–13759.
- (44) Bechelany, M.; Drobek, M.; Vallicari, C.; Abou Chaaya, A.; Julbe, A.; Miele, P. Highly Crystalline MOF-Based Materials Grown on Electrospun Nanofibers. *Nanoscale* **2015**, *7* (13), 5794–5802.
- (45) Chen, Y.; Li, S.; Pei, X.; Zhou, J.; Feng, X.; Zhang, S.; Cheng, Y.; Li, H.; Han, R.; Wang, B. A Solvent-Free Hot-Pressing Method for Preparing Metal-Organic-Framework Coatings. *Angew. Chem., Int. Ed.* **2016**, *55* (10), 3419–3423.
- (46) López-Maya, E.; Montoro, C.; Rodríguez-Albelo, L. M.; Aznar Cervantes, S. D.; Lozano-Pérez, A. A.; Cenís, J. L.; Barea, E.; Navarro, J. A. R. Textile/Metal–Organic-Framework Composites as Self-Detoxifying Filters for Chemical-Warfare Agents. *Angew. Chem., Int. Ed.* **2015**, *54* (23), 6790–6794.
- (47) Lu, A. X.; McEntee, M.; Browe, M. A.; Hall, M. G.; DeCoste, J. B.; Peterson, G. W. MOFfabric: Electrospun Nanofiber Mats from PVDF/UiO-66-NH₂ for Chemical Protection and Decontamination. *ACS Appl. Mater. Interfaces* **2017**, *9* (15), 13632–13636.
- (48) Neufeld, M. J.; Harding, J. L.; Reynolds, M. M. Immobilization of Metal–Organic Framework Copper (II) Benzene-1,3,5-tricarboxylate (CuBTC) onto Cotton Fabric as a Nitric Oxide Release Catalyst. *ACS Appl. Mater. Interfaces* **2015**, *7* (48), 26742–26750.
- (49) Yu, M.; Li, W. X.; Wang, Z. Q.; Zhang, B. W.; Ma, H. J.; Li, L. F.; Li, J. Y. Covalent Immobilization of Metal-Organic Frameworks onto the Surface of Nylon—a New Approach to the Functionalization and Coloration of Textiles. *Sci. Rep.* **2016**, *6*, 22796.
- (50) Lee, D. T.; Zhao, J.; Peterson, G. W.; Parsons, G. N. Catalytic “MOF-Cloth” Formed via Directed Supramolecular Assembly of UiO-66-NH₂ Crystals on Atomic Layer Deposition-coated Textiles for Rapid Degradation of Chemical Warfare Agent Simulants. *Chem. Mater.* **2017**, *29* (11), 4894–4903.
- (51) Zhao, J.; Lee, D. T.; Yaga, R. W.; Hall, M. G.; Barton, H. F.; Woodward, I. R.; Oldham, C. J.; Walls, H. J.; Peterson, G. W.; Parsons, G. N. Ultra-Fast Degradation of Chemical Warfare Agents Using MOF-Nanofiber Kebabs. *Angew. Chem., Int. Ed.* **2016**, *55* (42), 13224–13228.
- (52) Lee, D.; Zhao, J.; Oldham, C.; Peterson, G.; Parsons, G. UiO-66-NH₂MOF Nucleation on TiO₂, ZnO, and Al₂O₃ ALD-Treated Polymer Fibers: Role of Metal Oxide on MOF Growth and Catalytic Hydrolysis of Chemical Warfare Agent Simulants. *ACS Appl. Mater. Interfaces* **2017**, *9* (51), 44847–44855.
- (53) Rose, M.; Bohringer, B.; Jolly, M.; Fischer, R.; Kaskel, S. MOF Processing by Electrospinning for Functional Textiles. *Adv. Eng. Mater.* **2011**, *13* (4), 356–360.
- (54) Kalaj, M.; Denny, M. S., Jr; Bentz, K. C.; Palomba, J. M.; Cohen, S. M. Nylon–MOF Composites through Postsynthetic Polymerization. *Angew. Chem., Int. Ed.* **2019**, *58* (8), 2336–2340.
- (55) da Silva Pinto, M.; Sierra-Avila, C. A.; Hinestroza, J. P. In Situ Synthesis of A Cu-BTC Metal-Organic Framework (MOF 199) onto Cellulosic Fibrous Substrates: Cotton. *Cellulose* **2012**, *19* (5), 1771–1779.
- (56) Nakahama, M.; Reboul, J.; Kamei, K.-i.; Kitagawa, S.; Furukawa, S. Fibrous Architectures of Porous Coordination Polymers-Alumina Composites Fabricated by Coordination Replication. *Chem. Lett.* **2014**, *43* (7), 1052–1054.
- (57) Lee, D. T.; Jamir, J. D.; Peterson, G. W.; Parsons, G. N. Water Stable Chemical-Protective Textiles via Euhedral Surface-Oriented 2D Cu-TCPP Metal-Organic Frameworks. *Small* **2019**, *15* (10), 1805133.
- (58) Lee, D. T.; Jamir, J. D.; Peterson, G. W.; Parsons, G. N. Protective Fabrics: Metal-Organic Framework Textiles for Rapid Photocatalytic Sulfur Mustard Simulant Detoxification. *Matter* **2020**, *2*, 404–415.
- (59) Ma, K.; Wang, Y.; Chen, Z.; Islamoglu, T.; Lai, C.; Wang, X.; Fei, B.; Farha, O. K.; Xin, J. H. Facile and Scalable Coating of Metal–Organic Frameworks on Fibrous Substrates by a Coordination Replication Method at Room Temperature. *ACS Appl. Mater. Interfaces* **2019**, *11* (25), 22714–22721.
- (60) Lemaire, P. C.; Zhao, J.; Williams, P. S.; Walls, H. J.; Shepherd, S. D.; Losego, M. D.; Peterson, G. W.; Parsons, G. N. Copper Benzenetricarboxylate Metal-Organic Framework Nucleation Mechanisms on Metal Oxide Powders and Thin Films Formed by Atomic Layer Deposition. *ACS Appl. Mater. Interfaces* **2016**, *8*, 9514–9522.
- (61) Khanjani, S.; Morsali, A. Ultrasound-Promoted Coating Of MOF-5 on Silk Fiber and Study of Adsorptive Removal and Recovery of Hazardous Anionic Dye “Congo Red. *Ultrason. Sonochem.* **2014**, *21* (4), 1424–1429.
- (62) Dwyer, D. B.; Dugan, N.; Hoffman, N.; Cooke, D. J.; Hall, M. G.; Tovar, T. M.; Bernier, W. E.; DeCoste, J.; Pomerantz, N. L.; Jones, W. E., Jr. Chemical Protective Textiles of UiO-66-Integrated PVDF Composite Fibers with Rapid Heterogeneous Decontamination of Toxic Organophosphates. *ACS Appl. Mater. Interfaces* **2018**, *10* (40), 34585–34591.
- (63) Li, P.; Li, J.; Feng, X.; Li, J.; Hao, Y.; Zhang, J.; Wang, H.; Yin, A.; Zhou, J.; Ma, X.; Wang, B. Metal-Organic Frameworks with Photocatalytic Bactericidal Activity for Integrated Air Cleaning. *Nat. Commun.* **2019**, *10*, 2177.
- (64) Chen, Y.; Zhang, S.; Cao, S.; Li, S.; Chen, F.; Yuan, S.; Xu, C.; Zhou, J.; Feng, X.; Ma, X.; Wang, B. Roll-to-Roll Production of Metal-Organic Framework Coatings for Particulate Matter Removal. *Adv. Mater.* **2017**, *29*, 1606221.

(65) Ma, X.; Chai, Y.; Li, P.; Wang, B. Metal–Organic Framework Films and Their Potential Applications in Environmental Pollution Control. *Acc. Chem. Res.* **2019**, *52*, 1461–1470.

(66) Wang, H.; Rassa, P.; Wang, X.; Li, H.; Wang, X.; Wang, X.; Feng, X.; Yin, A.; Li, P.; Jin, X.; Chen, S.-L.; Ma, X.; Wang, B. An Iron-Containing Metal–Organic Framework as a Highly Efficient Catalyst for Ozone Decomposition. *Angew. Chem., Int. Ed.* **2018**, *57*, 16416–16420.

(67) Chen, Z.; Ma, K.; Mahle, J. J.; Wang, H.; Syed, Z. H.; Atilgan, A.; Chen, Y.; Xin, J. H.; Islamoglu, T.; Peterson, G. W.; Farha, O. K. Integration of Metal–Organic Frameworks on Protective Layers for Destruction of Nerve Agents Under Relevant Conditions. *J. Am. Chem. Soc.* **2019**, *141* (51), 20016–20021.

(68) Zhuang, J.-L.; Ceglarek, D.; Pethuraj, S.; Terfort, A. Rapid Room-Temperature Synthesis of Metal–Organic Framework HKUST-1 Crystals in Bulk and as Oriented and Patterned Thin Films. *Adv. Funct. Mater.* **2011**, *21* (8), 1442–1447.

(69) Ameloot, R.; Gobechiya, E.; Uji-i, H.; Martens, J. A.; Hofkens, J.; Alaerts, L.; Sels, B. F.; De Vos, D. E. Direct Patterning of Oriented Metal–Organic Framework Crystals via Control over Crystallization Kinetics in Clear Precursor Solutions. *Adv. Mater.* **2010**, *22* (24), 2685–2688.

(70) Mondloch, J. E.; Katz, M. J.; Isley III, W. C.; Ghosh, P.; Liao, P.; Bury, W.; Wagner, G. W.; Hall, M. G.; DeCoste, J. B.; Peterson, G. W.; Snurr, R. Q.; Cramer, C. J.; Hupp, J. T.; Farha, O. K. Destruction of Chemical Warfare Agents Using Metal–Organic Frameworks. *Nat. Mater.* **2015**, *14* (5), 512.

(71) Katz, M. J.; Mondloch, J. E.; Totten, R. K.; Park, J. K.; Nguyen, S. T.; Farha, O. K.; Hupp, J. T. Simple and Compelling Biomimetic Metal–Organic Framework Catalyst for the Degradation of Nerve Agent Simulants. *Angew. Chem., Int. Ed.* **2014**, *53* (2), 497–501.

(72) Peterson, G. W.; Moon, S.-Y.; Wagner, G. W.; Hall, M. G.; DeCoste, J. B.; Hupp, J. T.; Farha, O. K. Tailoring the Pore Size and Functionality of UiO-type Metal–Organic Frameworks for Optimal Nerve Agent Destruction. *Inorg. Chem.* **2015**, *54* (20), 9684–9686.

(73) Moon, S. Y.; Liu, Y.; Hupp, J. T.; Farha, O. K. Instantaneous Hydrolysis of Nerve-Agent Simulants with a Six-Connected Zirconium-Based Metal–Organic Framework. *Angew. Chem., Int. Ed.* **2015**, *54* (23), 6795–6799.

(74) Smith, M. K.; Mirica, K. A. Self–Organized Frameworks on Textiles (SOFT): Conductive Fabrics for Simultaneous Sensing, Capture, and Filtration of Gases. *J. Am. Chem. Soc.* **2017**, *139* (46), 16759–16767.

(75) Zhu, H.; Ka, B.; Murad, F. Nitric Oxide Accelerates the Recovery from Burn Wounds. *World J. Surg.* **2007**, *31* (4), 624–631.

(76) Wu, Y.; Zhou, Z.; Meyerhoff, M. E. In vitro Platelet Adhesion on Polymeric Surfaces with Varying Fluxes of Continuous Nitric Oxide Release. *J. Biomed. Mater. Res., Part A* **2007**, *81* (4), 956–963.

(77) Ferro, A. S-Nitrosothiols as Nitric Oxide-Donors: Chemistry, Biology and Possible Future Therapeutic Applications. *Curr. Med. Chem.* **2004**, *11* (20), 2679–2690.

(78) Harding, J. L.; Reynolds, M. M. Metal Organic Frameworks as Nitric Oxide Catalysts. *J. Am. Chem. Soc.* **2012**, *134* (7), 3330–3333.